MMWAVE PATH LOSS MODELING FOR 5G APPLICATIONS

Satzhan Askarov, B. of Eng. in Electrical and Computer Engineering

Submitted in fulfilment of the requirements for the degree of Master of Science in Electrical and Computer Engineering

School of Engineering and Digital Sciences
Department of Electrical and Computer Engineering
Nazarbayev University

53 Kabanbay Batyr Avenue,
Nur-Sultan, Kazakhstan, 010000

Supervisor: Prof. Refik Kizilirmak
Co-supervisor: Prof. Behrouz Maham

April, 2024

Declaration form

I hereby, declare that this manuscript, entitled “mmWave Path Loss Modeling for 5G Applications”, is the result of my own work except for quotations and citations which have been duly acknowledged.
I also declare that, to the best of my knowledge and belief, it has not been previously or concurrently submitted, in whole or in part, for any other degree or diploma at Nazarbayev University or any other national or international institution.

Name: Satzhan Askarov
Date: 05.04.2024

Abstract

This thesis examines the performance of outdoor communication systems, with special emphasis on the effects of adverse weather conditions like snowstorm, frequency bands, and modulation techniques Using Path Loss modeling through simulation and hardware experiments, thus this work provides a comprehensive insight into communicating mmWave's power challenges and capabilities in the field.

Findings from the path loss simulator within the Nazarbayev University (NU) campus territory highlight the importance of carrier frequency selection and modulation order in outdoor communication systems. Frequencies from higher bands cover less area due to higher path loss, which underlines the importance of frequency band selection. It is revealed that modulation order influences coverage area within line-of-sight (LOS) zones as well. Hence, those lower orders give more coverage and higher orders enable greater bandwidth efficiency. Recommendations on modulation techniques can be based on geographical considerations and the density and activity levels of users. In this regard, QPSK modulation can be preferred for harsh environments and long distances, and orders higher are appropriate for high data rate transmission in densely populated areas.

Hardware experiments in the 60 GHz mmWave channel are handled in indoor and outdoor environments during snowfall and windy weather. The received power is measured at different transmitter – receiver (T – R) distances and path loss results demonstrate similar to logarithmic growth for indoor and outdoor environments, yet the growth resembles exponential growth for distances larger than 7 meters in outdoor snowstorm circumstances. Outdoor path loss suffers more signal attenuation, which is conditioned by snow accumulation on antenna surface and the snowstorm environment itself. The path loss

exponent (PLE) values discovered during experiments constitued 4.12 for outdoor snowstorm conditions and 2.77 for indoor lab environment.

Repeated simulations using the obtained path loss parameters, i.e., PLE and shadow fading standard deviation inherent to snowy weather conditions illustrates considerable losses in coverage compared to the initial theoretical simulations. The work underscores the impracticality of the assumption that solely using base stations as uniform circular antenna arrays with omnidirectional transmission capabilites may be sufficient for the mmWave channels at 60 GHz to maintain proper power coverage in outdoor environment, especially during during snowstorms. Hence, initiatives like relay base stations and beamforming technology can be extremely useful in improving network resilience and robustness.

Future extension of the work would include the following directions: improving base station designs from uniformly omnidirectional to circular sectorized cells; updating the digital NU campus map from 2D to 3D for more realistic and accurate simulations, and investigating advanced antenna placement strategies to shelter them from snowfall moisture without interfering their radiation pattern. Subsequent research should look on network traffic analysis to determine placement spots for the base stations and the needed number of them to effectively satisfy the user traffic demand under different modulation modes. Furthermore, to minimize the positive bias of the coverage results and to make them more realistic and useful, the campus map requires the integration of the building heights, so that the T – R distance parameter considers 3D T – R distance rather than 2D approximation.

Acknowledgments

I want to start by expressing my gratitude to my supervisors, Drs. Behrouz Maham, Ikechi Ukaegbu, and Refik Kizilirmak. Throughout the preceding two years, their guidance and oversight were very beneficial to me, enabling me to effectively navigate and finish my Master's degree. I am grateful for the many hours of fascinating guidance they have kindly given, especially on mmWave technology and communication.

Second, for financial support of this work, I would like to thank the Nazarbayev University Faculty Development Competitive Research Grant Programme (grant no. 20122022FD4125), Scientific and Technical Projects (AP13068587, AP14871109), which are funded by the Ministry of Education and Science of the Republic of Kazakhstan, and the Nazarbayev University Collaborative Research Project (grant no. 11022021CRP1507).

Third, special thanks to Prof. Kizilirmak, Prof. Shafiee, Israel Ehile, Abubakar Abdulkarim, Daryn Shaldybayev, Kozhakhmet Abdugapbar, and Yernur Kalikhan for assisting experiments in windy and cold weather crucial for my thesis.

Lastly, my sincere gratefulness to the One who deserves all praises, gratitudes, and glory. Alhamdulillah.

Table of Contents

List of Abbreviations

BS	Base Station
dBm	Decibel milliwatt
FSPL	Free Space Path Loss
HPBW	Half Power Beam Width
LOS	Line – Of – Sight
NLOS	Non – Line – Of – Sight
PLE	Path Loss Exponent
QAM	Quadrature Amplitude Modulation
QPSK	Quadrature Phase Shift Keying
RX	Receiver
SF	Shadow Fading
SNR	Signal – to – Noise Ratio
TX	Transmitter

Chapter 1 – Introduction

1.1 General

Millimeter wave, also known as mmWave, is a range of radio frequencies in the electromagnetic spectrum that are extremely high in frequency and very short in wavelength. They are higher in frequency than the radio waves used for traditional wireless communication and are typically in the range of 30 to 300 GHz, which corresponds to the range of 1 millimeter to 10 millimeters. Having much wider bandwidths than traditional frequency bands, they can enable considerably high-speed wireless networks [1]. However, due to their nature, mmWave bands are easily blocked or reflected by obstacles, resulting in significant power losses and due to inherent large free space path losses, they have reduced signal coverage [2]. MmWave signals are also affected by weather conditions such as rain, fog, and snow, which can further reduce signal power and coverage. Hence the use of mmWave bands presents significant challenges that must be addressed to ensure the reliable and effective operation of future 5G wireless networks. The study in [3] indicates that at frequencies of 28 and 73 GHz it is feasible to achieve considerable coverage at the street level up to about 200 meters from a low-power base station, even in an urban canyon setting where a direct path between the transmitter (TX) and receiver (RX) is not possible. Hence, by careful examination of mmWave channels and an attentive approach to mmWave network design and deployment, it is possible to realize the full potential of the mmWave spectrum for high-speed wireless communication systems.

At the heart of mmWave research is specialist expertise and the optimization of numerous critical materials and processes. These include free space path loss (FSPL), which explains the attenuation of electromagnetic signals as they flow through open space without any barriers. FSPL is a fundamental concept in wireless communication design, particularly in

understanding how signal strength drops over time over a T - R distance from the TX network to the RX (see Eq. 4).

Another important concept associated with the mmWave research area is the Path Loss Exponent (PLE), which defines the rate at which signal strength decays with increase in T – R distance. To make mmWave communication systems simpler to design that would work stable over large T – R separation distances and in various unfavorable conditions, it is crucial know how to precisely predict and model the path loss, which is not possible without knowing the PLE inherent to a certain environment. In addition, the Shadow Fading (SF) phenomenon also spots light on distinct limitations of the mmWave spectrum. SF is defined as fluctuations of a signal envelope due to large boundaries like as buildings, timber, snowfall, vegetation, or landscape characteristics that may obstruct or disperse the propagation of the signal. To maintan reliable communication in such dynamic outdoor environment it is important to cope with the SF impact.

On top of that, to evaluate the quality of channels in mmWave communication systems, another important factor or criterion signal-to-noise ratio (SNR) is used. In communication systems, it is a benchmark to calculate the power ratio of a desired signal to the strength of background noise in the communication channel. The ratio is usually given as a single numerical number in decibels (dB). The ratio may be zero, positive, or negative. A signal-to-noise ratio higher than 0 dB implies that the signal level exceeds the noise level. The signal quality improves as the ratio increases. Hence, as SNR increases the stronger and clearer the signal becomes compared to noise, which is crucial for improved communication quality and reliability. Noise is defined as any undesired disruption that impairs the intended signal's quality. It may contain thermal, quantum, electrical, impulsive, and intermodulation noise, among other things. Environmental elements such as temperature and humidity may also have an impact on noise levels.

Finally, it is pertinient to note that mmWave technology research is critical for developing long-lasting, dependable, and high-data-rate communication systems that can satisfy the increasing needs of today's wireless networks. In this regard, rigorous path loss analysis might be a very important tool for developing and mastering mmWave systems.

1.2 Aims & Objectives

Path Loss (PL) behavior investigation of the 60 GHz mmWave channel in both indoor and outdoor settings being subjected to harsh weather conditions is one of the primary research goals of this work. Since Astana’s cold and snowstorm weather conditions provide considerable obstacles for 60 GHz wireless communication systems, the focus is on finding the Path Loss Exponent (PLE) and Shadow Fading (SF) propagation parameters inherent to such unfavorable weather settings. To build dependable networks, it is necessary to have a thorough knowledge of how severe weather impacts signal transmission. This knowledge could shed light on how mmWave communication systems operate in practice.

Furthermore, the study aims to simulate the performance of the Line-Of-Sight (LOS) coverage based on PL of different mmWave band channels across the Nazarbayev University, specifically 28 GHz, 60 GHz, and 73 GHz, as well as various modulation modes, including Quadrature Phase Shift Keying (QPSK), 16-Quadrature Amplitude Modulation (QAM), and 256-QAM. The minimal required signal-to-noise ratio (SNR) per each modulation mode shall be utilized as a primary criterion of the LOS coverage. The objective of the LOS coverage simulator is to do a comparative analysis of the LOS coverage performance of different modulation modes at different transmission bandwidths.

In conclusion, the research attempts to resimulate the NU territory's LOS coverage performance based on the acquired PL parameters (PLE and SF standard deviation) of both indoor and outdoor situations at 60 GHz in the aforementioned three distinct modulation

modes. The resimulation aims to gain insight into how coverage might act in more realistic situations—primarily in severe weather and clear sky conditions.

1.3 Thesis structure

The study is arranged in the following manner: Chapter 2 covers the literature review, which discusses the challenges and the state-of-the-art of the mmWave technology. Chapter 3 includes an in-depth discussion of the hardware setup of the 60 GHz mmWave channel and the simulation model utilized in this study. Chapter 4 presents the results of the PL experiment along with the LOS coverage performance at 3 different bands and 3 different modulation modes. It also includes a detailed discussion on grounds as well as the deductions of the results obtained. Chapter 5 provides the general conclusion of the paper.

Chapter 2 – Literature Review

2.1 Penetration Loss measurements

Although mmWave technology can offer significant benefits, due to its shorter wavelength, mmWave spectrum has a high LOS propagation Free-Space Path Loss (FSPL). In addition, they suffer from greater Non-Line-Of-Sight (NLOS) penetration losses compared to lower frequency bands, which can have a serious impact on network coverage [4]. Therefore, it is important to investigate the penetration loss caused by various building materials at mmWave bands in NLOS scenarios. One of the main challenges to address associated with mmWave frequencies is the loss of signal when it penetrates from outdoors to indoors. One study by Du et al. examined how 28 GHz wideband mmWave signals behave at Johnston Regional Airport in outdoor, indoor, and indoor-to-outdoor scenarios [5]. The results on the LOS propagation, penetration, reflection, and signal coverage indicate that there is less path loss indoors, more scattering, and greater coverage compared to outdoors. Additionally, the authors noted that indoor-to-outdoor propagation losses are higher. Zhao et al. measured walls and buildings' reflections and penetration losses for different materials like brick, concrete, drywall, tinted glass, and clear glass at 28 GHz [6]. Results obtained indicated that outdoor building materials are exceptional reflectors, with tinted glass having the highest reflection coefficient of 0.896.

2.2 Path Loss measurements

Aside from substantial attenuation while passing through the materials, the small wavelength of mmWave frequencies leads to propagation challenges also counting significant FSPL [3]. Xu et al. examined the indoor channel at 60 GHz using a directional horn antenna on the RX side. They also used an open-ended waveguide with a 90-degree azimuth plane HPBW and a gain of 6.7 dBi at the TX [7]. The results obtained in indoor environments for

mmWave frequencies are similar to those observed for lower frequencies and the authors suggest that the reason the measured path loss is lower than the theoretical FSPL is attributed to the reflections from the ground and ceiling, as well as a waveguide effect, which increases the power received by the RX. In the study by Du et al., theoretical FSPL is compared to LOS FSPL [5]. It can be seen that indoor FSPL agrees with the theoretical FSPL, but the outdoor path loss is around 2-3 dB greater than indoor path loss. Also, besides both FSPLs, they are juxtaposed with the FSPL results of large-scale omnidirectional FSPL models by 3rd Generation Partnership Project (3GPP) Technical Report 38.901 [8] and Millimeter-Wave Based Mobile Radio Access Network for 5G Integrated Communications (mmMAGIC) [9] standards, as well as, of a research group at New York University (NYU) [10]. The indoor FSPL is higher by a few dB than the LOS omnidirectional indoor office models from 3GPP and mmMAGIC. However, the Rural Macrocell (RMa) model from NYU provided a better fit. Further discussion on FSPL can be done separately for indoor and outdoor scenarios, as mmWave behavior varies much in different environments.

2.2.1 Indoor Path Loss

In [11] experiments are conducted at 26 GHz and 38 GHz - frequencies that are significant for 5G mmWave communication - in both an indoor corridor and stairwell. The results showed that the stairwell had larger path loss exponents and Root-Mean-Square (RMS) delay spreads compared to the corridor, indicating a more challenging propagation environment. The study in [12] introduced a mmWave and sub-THz frequency statistical channel model in both LOS and NLOS conditions, conducting experiments in an office at 28 and 140 GHz. The channel statistics obtained revealed that the number of time clusters and subpaths within each cluster declined with increasing frequency. Wen et al. designed the mmWave channel sounder system utilizing offthe-shelf equipment and the suggested

structure, capable of accommodating up to 44 GHz, and 1 GHz bandwidth, and supporting both 4x4 single-input-single-output and multiple-input-multipleoutput settings [13]. They performed an indoor open office channel measurement campaign using the suggested mmWave channel sounder system at 26 GHz with 1 GHz bandwidth, yielding different LOS and NLOS channel measurements.

2.2.2 Outdoor Path Loss

Some researchers have carried out thorough campaigns for measurement in the mmWave bands to comprehend propagation attributes and assess its potential for the advancement of 5G communication systems. To precisely model the mmWave bands, they gathered data on key factors such as FSPL, delay spread, number of multipath components, and angles of arrival and departure (AoA and AoD), which would aid engineers in modeling the future Extremely High Frequency (EHF) wireless systems [1], [14]. FSPL for outdoor NLOS environments can be loared by using directional antennas with beamforming and combining the best directional links between TX and RX [15]. In their paper, MacCartney et al. [3] examined the suitability of E-band (60 GHz – 90 GHz) frequencies for backhaul and mobile wireless communication channels. Their measurement campaign showed that the use of on-chip antenna arrays and steerable antennas can help to achieve reliable radio links by manipulating the environment rich in multipath with beam combining and beamforming. The authors suggest that compact basestation units can be employed to launch mmWave consumer and backhaul connections on every street corner or lamppost in metropolitan areas.

2.3 System Coverage

Assessing the impact of building-related path loss in mmWave signals holds substantial promise for refining the design strategies of mmWave base stations (BS) or access

points. Through a thorough examination of signal obstruction and path loss associated with town buildings, there exists an opportunity to strategically position and configure network infrastructure, aiming to maximize coverage while minimizing areas with compromised connectivity. In university settings, characterized by high-density populations reliant on wireless connectivity for diverse needs, particularly around student dormitories, conventional cellular networks may face significant traffic demands. Leveraging mmWave technology presents an avenue for accommodating high-capacity, low-latency connections as a viable solution [16][17]. An understanding of building-induced path loss is crucial in ensuring consistent and dependable mmWave coverage, thereby ensuring a seamless user experience throughout the campus [18]. According to the the simulation results by Kim et al., there is a strong correlation between antenna configurations—including arrangement, tilting angle, and spacing— and the coverage and capacity of the mmWave channe. Generally, antennas emitting wide beams are found to extend system coverage, while those with narrow beams are observed to enhance channel quality and system capacity through alleviating the interbeam interference [19]. According to Tuovinen et al., achieving data rates close to 10 Gbit/s requires multiple several spatially multiplexed data streams for each user. Their study covers analysis of signal processing, antennas, RF impairments, and radio propagation to analyze the link budget for 5G mmW multiantenna systems [20].

Chapter 3 –Path Loss Simulator

3.1 Methodology

3.1.1 Path Loss simulator for the NU campus

The path loss simulator assesses how well the mmWave signals at a certain band and modulated in a certain mode covers the LOS territory of the Nazarbayev University campus around the base stations in Astana. The simulation principle is based on the minimal SNR and the classic Path Loss equations as pivotal measures.

3.1.2 Design and Implementation of the Simulator.

Initially, the satellite Campus Map is exported from the Google Earth Pro app dated June 2023 (Figure 1). The map first is cleaned manually so that only the buildings' contour remains (Figure 2). Then the map went through Matlab preprocessing using the colorThresholder tool to obtain the binary (black and white) map (Figure 3).

Fig. 1. Sattelite image of the NU campus

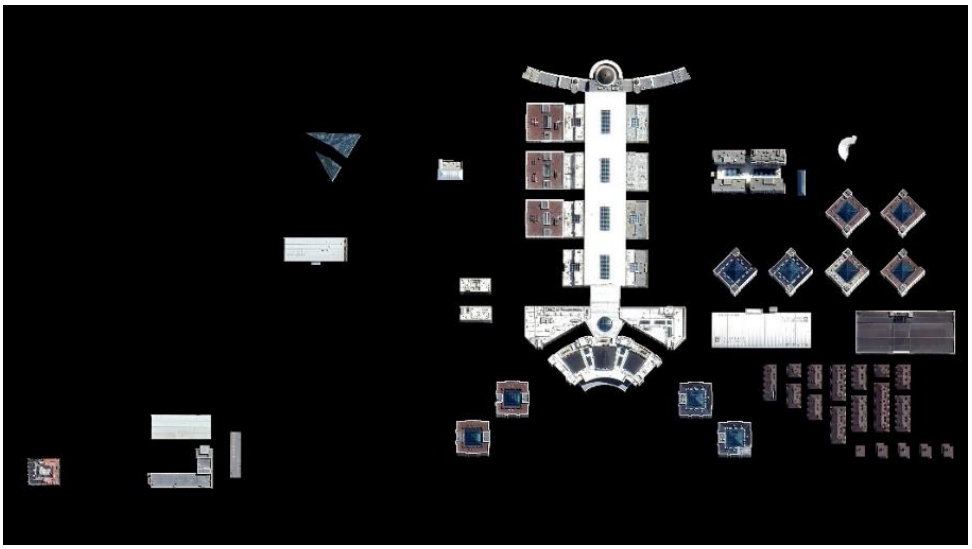

Fig. 2. Cleaned campus map

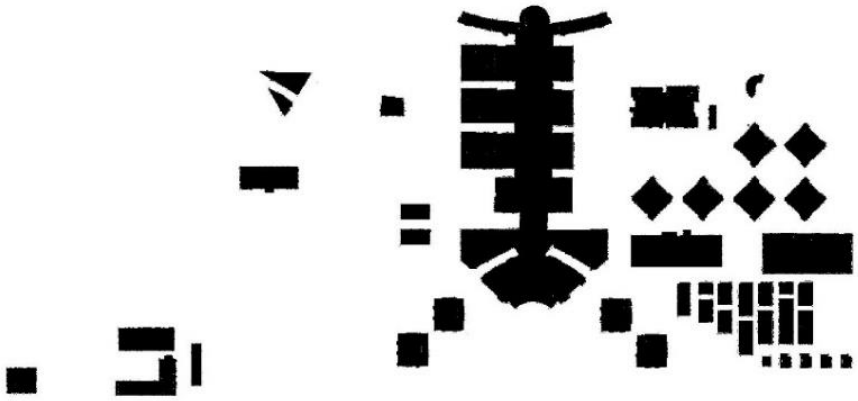

Fig. 3. Binary campus map

Simulations are carried out with 4 arbitrarily placed BSs. The 4 BSs are positioned on the corners of building rooftops, assuming a downlink channel of 1 GHz bandwidth within the specified band. The BS locations are selected to cover areas with potentially large density of 5G network users. By employing a top-down viewpoint obtained from satellite imagery, it was possible to evaluate the geometric line-of-sight coverage performance for mmWave channels realistically. Nevertheless, the lack of building height data in Google Earth Pro for Astana imposed a limitation on the simulator, necessitating the

presumption of consistent building heights that also were considerably greater in height than the transmitter antenna. This restriction may largely influence the results' accuracy due to rounding the actual 3D distance from the base station to a test point via a 2D distance since the power attenuation rate of the signal at mmWave bands is highly susceptible to T – R distance. However, for the sake of the comparative analysis of the different mmWave channels' performance under different modulation modes, the approximations are quite acceptable. Leveraging the present geospatial information, the simulation models wireless mmWave channels coverage based on minimum required SNR and LOS principles [18].

The dimensions of the campus territory considered for this research in the retrieved map are also retrieved from Google Earth Pro, which constituted 705 meters in width and 1292 meters in length to the nearest half meter. The corresponding amount of unit pixels in width and length are retrieved as well, which constituted 4586 and 8192 pixels, repectively. However, they did not match the actual T – R distance dimensions scale, i.e., the T – R distance to pixels ratio in width and length are not the same due to the non-quadratic size of a unit pixel. Hence, to define this fundamental ratio of T – R distance to pixel, the mean of 2 separate ratios in width and length is considered. Utilizing this ratio, the number of pixels in a 10-meter segment is found and the binary map of the campus is examined as a grid of cells with dimensions of 10 meters by 10 meters. The simulator checks whether the RX power at each vertice of 10 meters by 10 meters cell is sufficient for the signal under consideration to be valid (Figure 4). Overall, the grid of cells is 127 vertices long and 71 vertices wide, meaning there are a total of 9017 vertices. The validity of RX power from each BS is checked upon each vertice, meaning the RX power calculations are done in overall $9017 \times 4 = 36068$ times.

For any cell vertice within the NU campuss binary map to receive a valid signal, it requires an LOS path to any BS and an SNR meeting or exceeding the minimum required

SNR for the modulation order being considered. LOS path means that there is no black pixel along the line that stretches from a BS to the vertice under the test, which is possible to detect using the *improfile* MATLAB function. The minimum SNR requirements for each modulation order at a coding rate of 1/2 are detailed in Table I. The simulator utilised a path loss (PL) model to account for the mmWave channels operating at 28GHz, 60GHz, and 73GHz., i.e., how much the signal power will be attenuated when broadcasting at a certain frequency to a certain distance is determined by the classic equation:

$$\text{PL} = 10 \times \log_{10}(\frac{4\pi f}{c})^2 + 10 \times n \times \log_{10}(\frac{d}{d_0}) \qquad (1)$$

Here, f represents the signal's carrier frequency, c denotes the speed of light, n stands for the path loss exponent (PLE), set at a free space value of n = 2 [3], the reference distance d_0 is established at a standard of 1m, and d signifies the *2D* distance between the BS and the testing vertice. The SNR at a testing point is subsequently calculated as:

$$\text{SNR} = \text{P}_{\text{TX}} - \text{PL} - (10 \times \log_{10}(kT_0B) + NF) \qquad (2)$$

In Eq. 2, P_{TX} stands for the transmitter (TX) power, set at 30 dBm for the uniform circular antenna array BS, k represents the Boltzmann constant ($1.38065\times10^{-23}\text{m}^2\text{kgc}^{-2}\text{K}^{-1}$), T0 denotes the nominal temperature (290K), B is the bandwidth (1GHz), and NF refers to the noise figure, assumed to be 10 dB [20]. The assumption is made regarding the PLE value, setting it at ideal value of 2 based on [3].

These two equations allowed me to gather the matrix with received power values for 9 different scenarios, considering each combination of 3 different frequency bands and 3 different modulation modes. To numerically quantify the valid signal coverage, it is presented as a percentage of the total LOS region achievable with the arbitrarily established BS locations. The total LOS area in the scope of this study is the area that could be covered

with the valid signal by all base stations having an infinite gain that extends to all possible areas within an LOS region and is limited by the NU campus territory. To find the coverage percentage, the sum of the vertices having valid signal is simply divided by the total number of vertices within the total LOS region and multiplied by 100%.

Table 1. Minimum SNR thresholds for different modulation techniques at code rate 1/2

Modulation	QPSK	16-QAM	256-QAM
SNR_{min} threshold	7.0dB	14.5dB	27dB

Initially, employing Eq. 2, the SNR matrices are derived from Received Power matrices. Subsequently, within each of the 9 cases, the SNR matrices are purged of values set to –inf, retaining solely authentic SNR values, indicating the valid points where the mmWave signal is present. These values are then organized into a row vector and arranged in ascending order. The mean and standard deviation for each vector are computed. Lastly, by processing the refined SNR vectors alongside their mean and standard deviation via *evcdf* function in Matlab, a vector representing cumulative probabilities corresponding to each SNR value in the SNR vector is generated.

3.2 Simulation Results

3.2.1 Simulation results presentation

The simulation per each particular scenario lasted on average for about 5600 seconds, which corresponds to 93 minutes. Table 2 displays the campus coverage simulation results. It shows what proportions of the total LOS area are covered across various frequency bands and modulation orders. The LOS area covered by the chosen base station

placements accounted for 47.10% of the entire outdoor area of the NU campus. At a carrier frequency of 28 GHz, both QPSK and 16-QAM signals cover the entire LOS region. However, when moving to 256-QAM, the coverage drops notably to 41.98% of the total LOS regions. At 60 GHz, QPSK maintains complete LOS coverage, but 16-QAM and 256-QAM drop to 88.32% and 13.21% coverage, respectively. The most significant decrease occurs at 73 GHz, where despite QPSK covering most LOS areas, higher modulation orders, especially 256-QAM, dramatically reduce coverage, reaching as low as 9.42%. To enhance the clarity and understanding of the simulator algorithm and the signal coverage in the geometrical sense, an exemplary dot-contoured grid with 10-meter unit cells, representing the coverage at 28 GHz with 256-QAM modulation is provided in Figure 4. In this contour, the green circles imply the vertices where the RX power or the corresponding SNR ratio are valid, and accordingly, red x-marks mean either NLOS sites or vertices that do not meet the minimum SNR requirements.

Table 2. The percentage of Line-of-Sight (LOS) area covered by the signal in each scenario.

	QPSK	**16-QAM**	**256-QAM**
28GHz	100%	100%	41.98%
60GHz	100%	88.32%	13.21%
73GHz	99.93%	74.83%	9.42%

Coverage areas for the 28 GHz, 60 GHz, and 73 GHz bands at three different modulation levels are shown in Figures 5, 6, and 7, respectively. In these figures, the green dashed contour defines the area allowing transmission for the 256-QAM signal. Likewise, the blue dashed and yellow dashed contours represent covered regions for 16-QAM and QPSK, respectively. Figure 6 specifically displays coverage areas for the 60 GHz band,

revealing that QPSK (blue contour) exhibits the broadest coverage, followed by 16-QAM (red contour). Notably, there is a reduced coverage area for 256-QAM compared to the 28 GHz band, in accordance with the anticipated increase in path loss with the increase in frequency.

Figures 8 – 10 display the CDF distributions of SNRs for three distinct modulation orders within the 28 GHz, 60 GHz, and 73 GHz bands, respectively. The CDF distributions cover those SNR levels across the campus area which are larger than equal to the minimum required SNR level for the considered modulation mode and at each of the three frequency bands (28, 60, and 73 GHz). Figure 8 depicts the CDF of SNR values across the LOS area for the 28 GHz channel. In areas covered by QPSK and 16-QAM, the SNR follows a similar distribution. Concerning the coverage of 256-QAM, however, over fifty percent of the measurement points have SNRs greater than 31 dB, beginning with the minimum required SNR of 27 dB. QPSK mode SNR CDF at 60 GHz starts from a 9.73 value, which matches with the QPSK mode coverage of the LOS region being 100% as noted in Table 2, since the minimum required SNR for this mode is 7dB. The 256-QAM mode resembles more or less the same pattern as in the 28 GHz channel, but with a little shift to the left, since with an increase in frequency the number of vertices that do not meet the required limit increases, due to what the probability of the nodes with relatively high SNR among those that passed the limit drops, as well. In addition, the 16-QAM mode now starts from exactly an SNR of 14, making some RX points fall below this limit, hence reducing the LOS coverage to 88.32%. The same trend is observed in the 73 GHz channel case, as the QPSK and 16-QAM plots shift somewhat to the left due to the decrease in the ceiling value i.e., the one that is at the 100-percentile, meaning all of the rest values are lower. This depreciation of the 100-percentile ceiling SNR has taken place obviously because of an increase in the channel band, as those nodes close to base stations having the

highest SNRs in 60 GHz now have lower maximums owing to larger path losses. As for the 256-QAM, the plot has seen an almost inconsiderable left shift, as the number of nodes satisfying the valid signal condition at this higher order of modulation at 60 GHz has inconspicuously decreased at 73 GHz, as this band is considerably closer to 60 GHz than the 28 GHz.

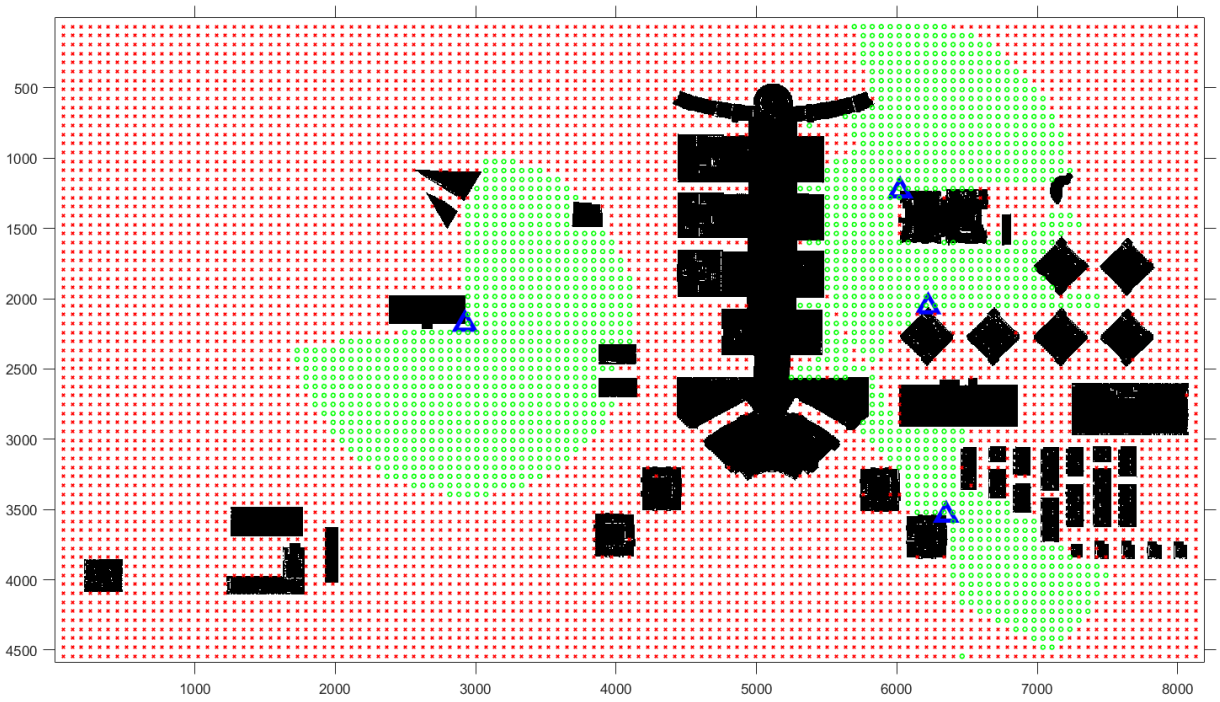

Fig. 4. RX power dot-contour for the 28 GHz channel and 256-QAM modulation

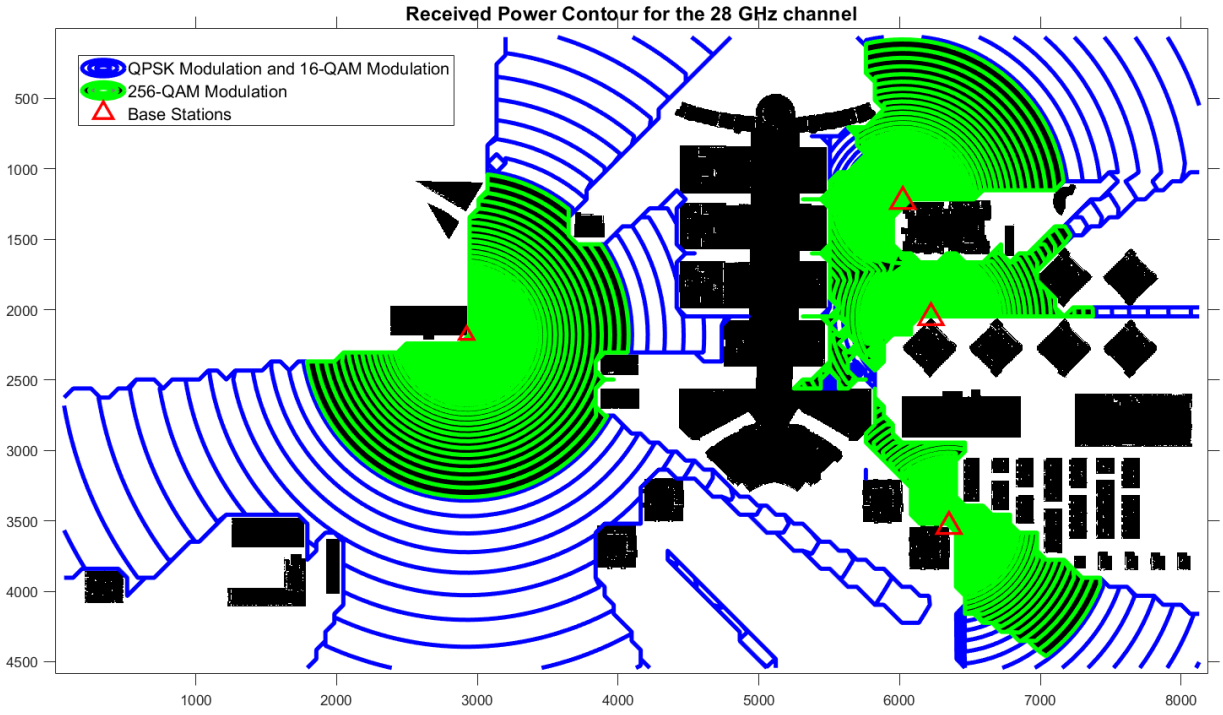

Fig. 5. Received Power Contour for the 28 GHz channel

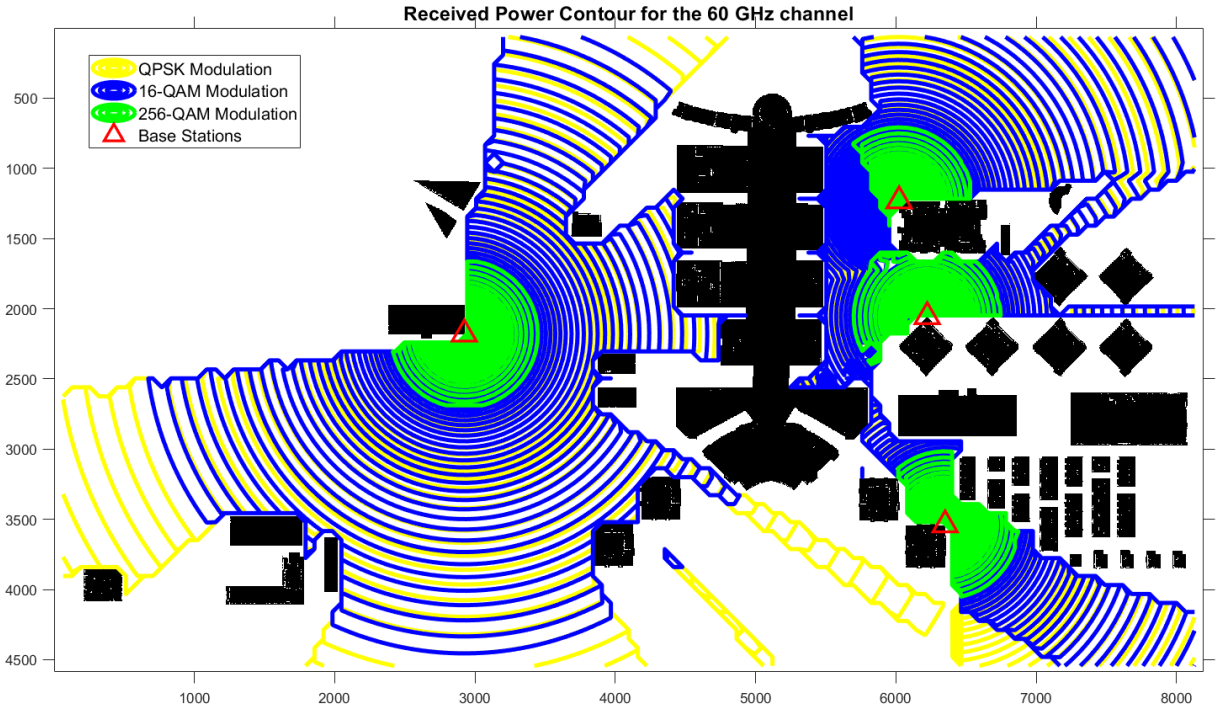

Fig. 6. Received Power Contour for the 60 GHz channel

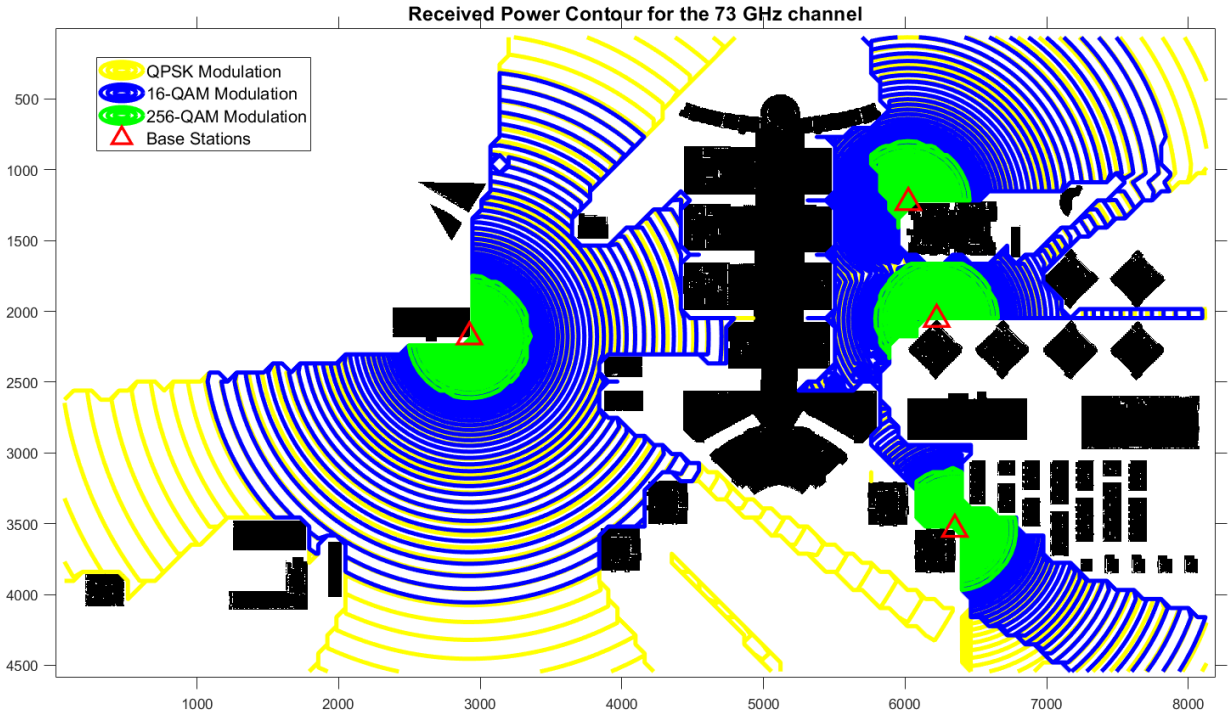

Fig. 7. Received Power Contour for the 73 GHz channel

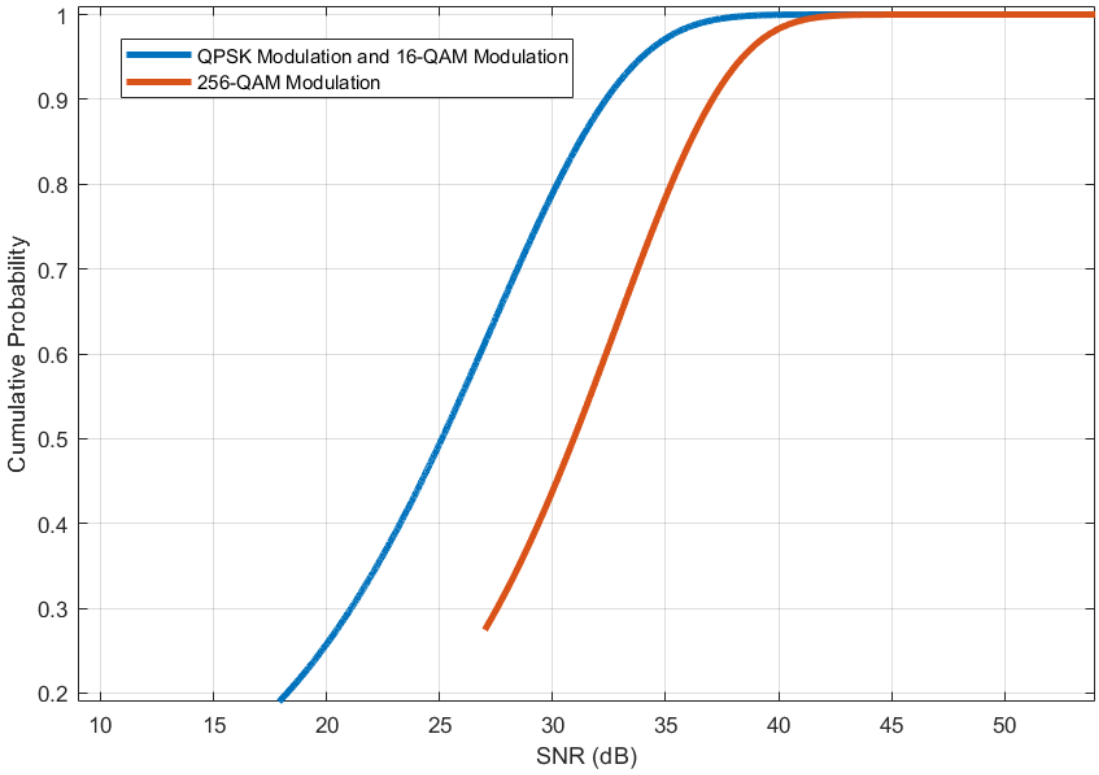

Fig. 8. SNR CDF for the 28 GHz channel

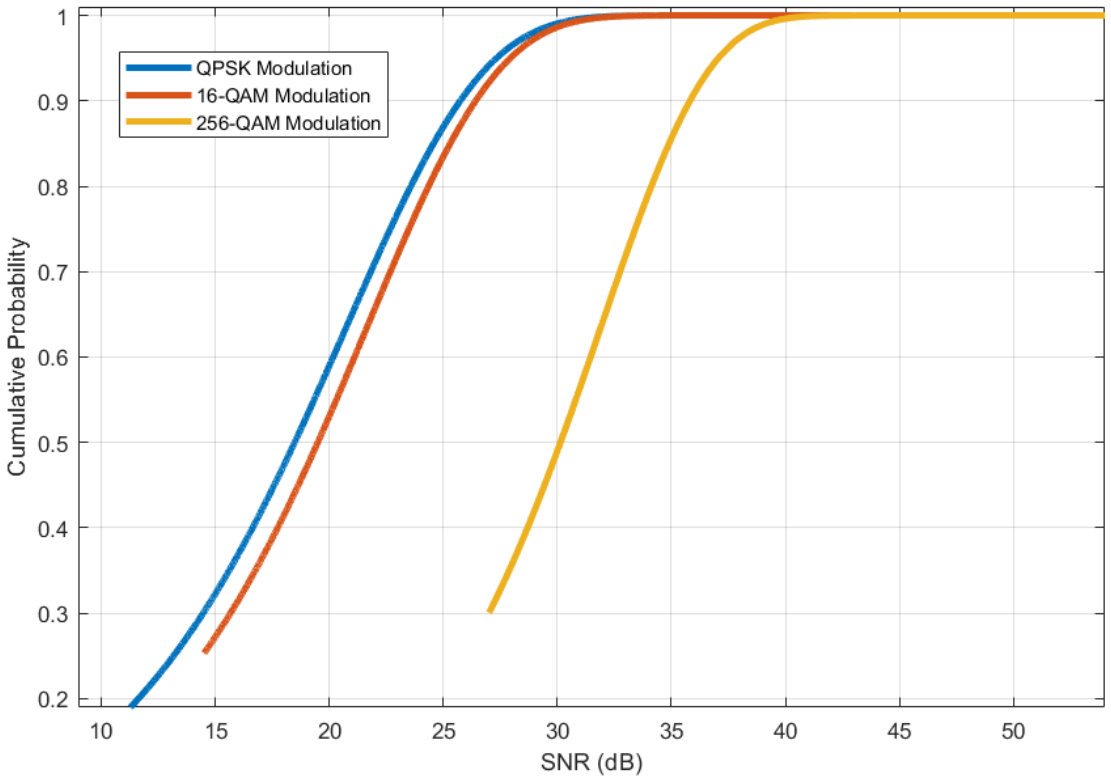

Fig. 9. SNR CDF for the 60 GHz channel

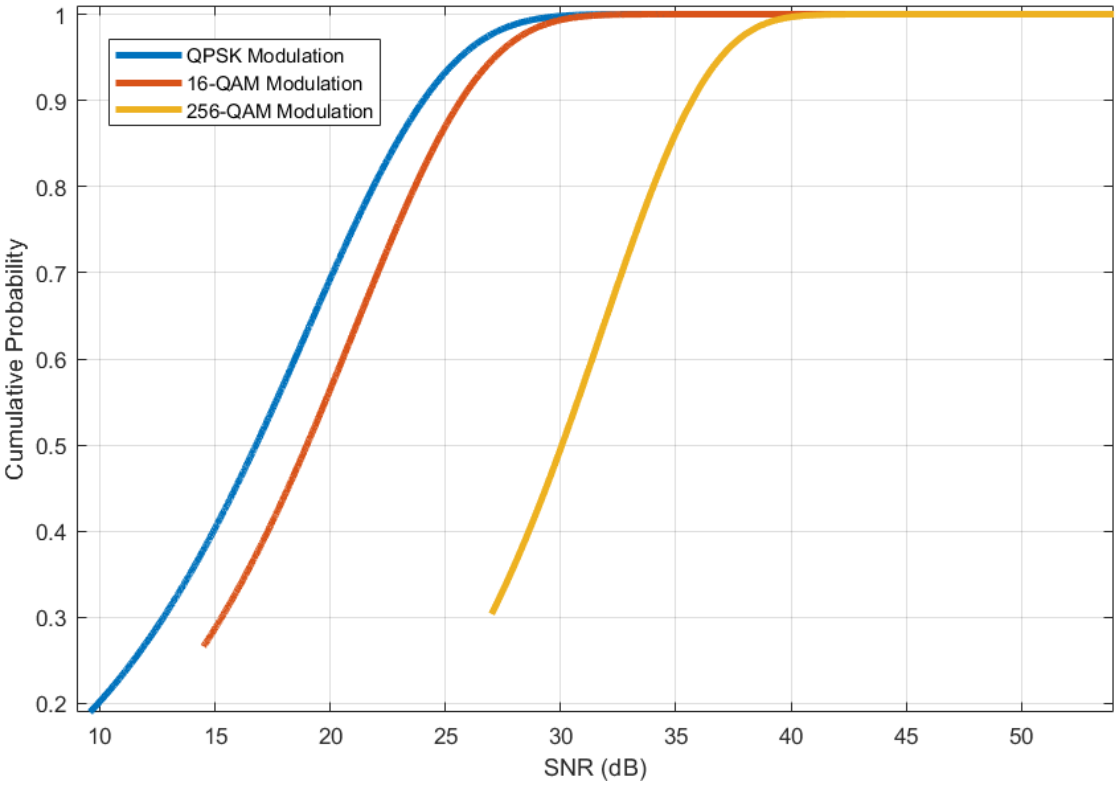

Fig. 10. SNR CDF for the 73 GHz channel

3.2.2 Simulation results discussion

The findings of the campus coverage simulation provide valuable insights into the performance of various frequency bands and modulation schemes for outdoor communication on the NU campus. The findings show how carrier frequency influences coverage. The valid signal coverage degrades with the increase in the frequency band. For example, at higher frequencies like 60 GHz and 73 GHz, coverage for all modulation orders is significantly lower than in the 28 GHz range. This decline is attributed to the legitimate increase in path loss at higher frequencies (See Eq. 5), emphasizing that path losses in the mmWave band are largely affected by the chosen carrier frequency and the necessity of frequency selection in outdoor communication systems. The RX power contour plots also draw insights into the influence of the T – R distance on path loss and therefore the RX power. The reduction in contour density i.e., the signal quality with a distancing from the signal source can be naturally inferred from Eq. 5. The simulator also examined the effect of modulation order on coverage area inside LOS areas. Results show that, while QPSK provides 100% LOS coverage across all frequency bands, higher modulation orders have gradually lower coverage. This trend highlights the importance of choosing the right modulation order based on the specific application needs and environmental factors. Understanding the signal quality at three frequency bands and modulation orders across the campus area provides valuable insights into the distribution of SNR values. The SNR analysis shows that the SNR distributions do the left shift with an increase in modulation order and frequency, indicating a decrease in the maximum SNR value. All in all, the MATLAB SNR matrices per each modulation order and frequency band can help influence judgments on receiver sensitivity, error correction techniques, and overall system performance improvement. Lower modulation orders like QPSK and 16-QAM provide wider LOS coverage but opting for a higher modulation order such as 256-QAM leads to significant reductions in coverage. This

underscores the importance of considering the trade-offs between data rate and coverage area. Higher data rates come at the cost of decreased coverage.

Acknowledging that QPSK modulation could offer better performance in more challenging environments or for longer BS–user distances, 16-QAM, and 256-QAM modulation modes could be preferred for high data rate communication in a restricted territory, especially in the mmWave spectrum. Among QPSK, 16-QAM, and 256-QAM, 256-QAM offers the largest bandwidth efficiency, meaning it can transmit the highest number of bits per symbol, i.e., 8 bits per symbol since 256-QAM can represent 256 different amplitude-phase combinations. In comparison, 16-QAM can transmit four bits per symbol, and QPSK can transmit two bits per symbol. Seeing that the green region around the lower-right and center-right base stations covers an appreciable portion of the dormitory and townhouse territory even at the 73 GHz band (Figure 7), which are the most densely populated areas of the university campus, the highest modulation order could be preferred to meet the high user traffic. By the same token, QPSK mode could be sufficient to cover the distant campus areas with potentially low population density (around Stella, Pyramid, and below the Technopark), as its coverage is noticeably larger, and signals in the mmWave spectrum with limited bandwidth can still offer high data rate traffic for the limited number of users. Furthermore, with comparatively lower susceptibility to noise and distortion (SNR), the QPSK and 16-QAM modes can be seen favored in providing robust performance during winter periods as Astana is famous for its harsh weather and strong winds. As this simulation does not provide any insight into traffic analysis, further research will be needed to draw more secure conclusions on trade-offs amid the sites, the modulation types and the numbers of BS needed to effectively provide high-traffic connection in the outdoor areas of the campus.

As per the simulation duration of 93 minutes on average for each scenario, it is linked with the fact mentioned in 3.1.2 that the RX measurements and check for signal validity are

done 36068 times eacb during each simulation. This “Brute force” approach should be modified in the future using dynamic or greedy algorithms to reduce the number of unnecessary calculations, comparisons and assignments using editable tables. This may be necessary and may enable efficient time management when the number of BS increases.

Chapter 4 – Path Loss Measurements

4.1 Methodology

4.1.1 mmWave hardware system setup

To examine the mmWave spectrum, particularly at 60GHz frequency the setup depicted in Figure 11 is designed. This setup uses identical tranceivers on both the receiver (RX) and the transmitter (TX) sides. Each tranceiver consists of the following elements: the Voltage Controlled Oscillator (VCO), I/Q Mixer and the Horn Antenna. The system specifications for the 60 GHz mmWave system are provided in Table 3. The RX side held stationary, while the TX system travels away in both the indoor and outdoor experiments. Due to differing factory calibrations between the two 60 GHz VCOs, it is possible to detect the downconverted carrier signal using the Rohde&Schwarz Spectrum Analyzer, designed for bands between 2 Hz and 43.5 GHz with maximum analysis bandwidth of 8312 MHz. Hence, the downconverted baseband signal is drawn from the in-phase port of the mixer on the RX site and fed to the Spectrum Analyzer through 1.85mm (male) – to – 1.85mm (male) wire. Since the connector of the in-phase port of the mixer was SMA female, an SMA male – to – 1.85 female adaptor is utilized to transfer the downconverted signal to the spectrum analyzer.

Table 3. 60 GHz mmWave System Specifications

Equipment	**Features**
VCO	Carrier frequency 60 GHz Bandwidth 2 GHz Control voltage 8-10 V Waveguide loss 0.02dB Power Output 17dBm
IQ Mixer	LO-to-RF isolation loss 28dB RF-to-IF conversion loss 10dB
TX power	3.98 dBm (see Eq. 3)
TX Antenna	Gain 25 dBi 9^o E-plane HPBW 10^o H-plane HPBW Linearly Polarized
RX Antenna	Gain 25 dBi 9^o E-plane HPBW 10^o H-plane HPBW Linearly Polarized
The Spectrum Analyzer	Frequency range 2 Hz−43.5 GHz Max. analysis bandwidth 8312 MHz

Fig. 11. Path Loss indoor experiment

As per the system specifications, the VCO frequency can be adjusted anywhere between 59-61 GHz depending on a DC control voltage range of 8-10 Volts, respectively. Despite applying a 9V control voltage to both VCOs from the same output channel of the DC power supply to generate a 60 GHz carrier baseband signal at TX and downconvert in at RX, a signal at a frequency around 800-900MHz, which represents the intermediate frequency (i.e., the difference between the carrier signal frequency and the downconverting signal frequency), became detectable on the Spectrum Analyzer at RX site. For biasing procedures, both LOs are fed with the Supply voltage of 6V. For the sake of the surface-to-surface LOS alignment, a rechargeable powerful monochromatic green laser pointer is attached on the RX side at the same distance from the RX antenna center as the distance from the center of the test cardboard to the TX antenna center. The TX power is calculated by deducting the sum of the Waveguide (L_{WG}), RF-to-IF (L_{RF2IF}), and LO-to-RF (L_{LO2RF}) conversion losses from the VCO power output (P_{VCO}) and by adding up the TX antenna gain (G_{TX}) at the end:

$$P_{TX} = P_{VCO} - (L_{WG} + L_{RF2IF} + L_{LO2RF}) + G_{TX} \qquad (3)$$

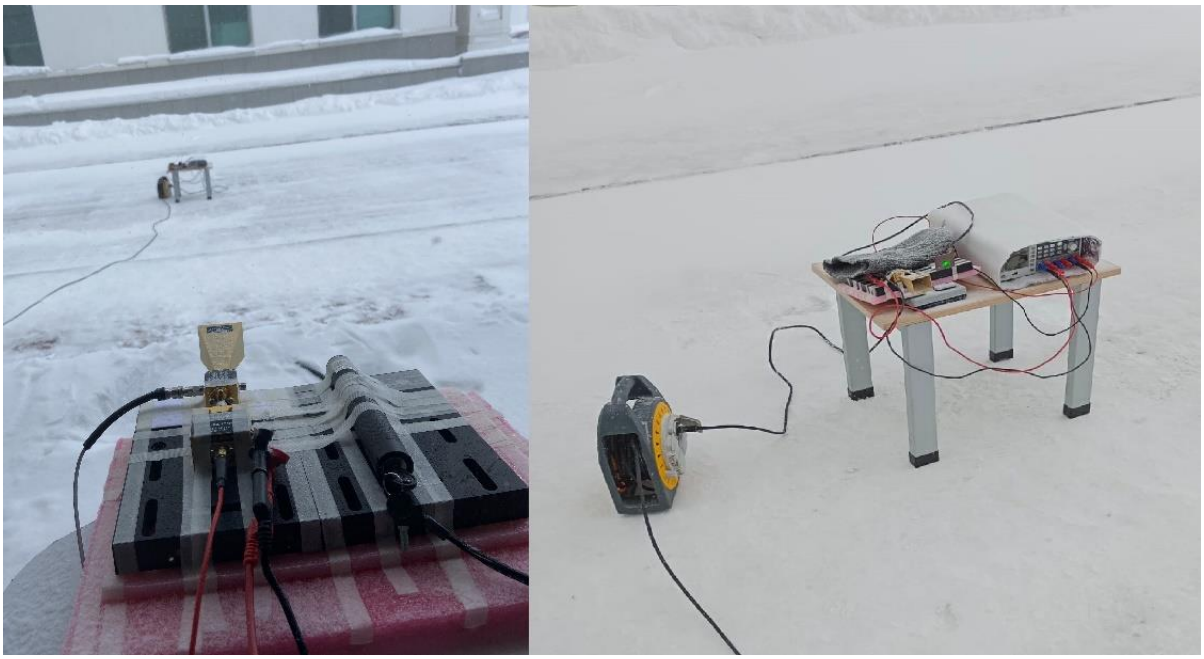

Fig. 12. Path Loss outdoor experiment

4.1.2 Path Loss Modelling

The ***close-in free space reference distance (CI)*** model is used to estimate the 60GHz mmWave channel path loss in both indoor and outdoor contexts due to its accuracy and ability to validate other models [21]. The symbol FSPL (f,1 m) represents the signal loss in free space, measured in decibels (dB), for a 3D T – R separation distance of 1 metre for the carrier frequency *f*, as shown in Eq. 4:

$$FSPL(f,1m)[dB] = 10log_{10}(\frac{4\pi f}{c})^2 \qquad (4)$$

where *c* is the speed of light. The CI model utilizes a reference distance of 1 meter, and it can be represented by Eq. 5:

$$X_\sigma^{CI} = PL^{CI}(f,d)[dB] - FSPL(f,1m)[dB] - 10nlog_{10}(d) = A - nD \quad (5)$$

Here, *n* represents the path loss exponent (PLE), *d* stands for the three-dimensional (3D) separation distance between the transmitter and receiver (3D T – R separation distance), and X_σ^{CI} signifies the SF factor that expresses the large-scale channel inconstancy, i.e., a zero

mean Gaussian random variable with standard deviation σ. Also, A (in dB) denotes $PL^{CI}(f,d)[dB] - FSPL(f,1m)[dB]$, and D implies $10log_{10}(d)$. To model the 60GHz mmWave channel for Astana's outdoor environment using CI model, the standard deviation of the SF and PLE value should be estimated using the experiment data, which can be achieved using Minimum Mean Square Error (MMSE) approach. Eq. 5 impllies that the standard deviation of the random variable X_{σ}^{CI} is:

$$\sigma^{CI} = \sqrt{\sum {X_{\sigma}^{CI}}^2/N} = \sqrt{\sum (A - nD)^2/N} \qquad (6)$$

In this context, *N* represents the quantity of path loss data points that have been measured. To perform these sums, the individual elements are added directly, meaning that if the elements are expressed in decibel (dB) units, the sum shall be computed by simply adding all the elements in dB units. To minimize the SF factor's standard deviation σ^{CI} the expression $\sum (A - nD)^2$ can be minimized by equating its derivative with respect to *n* to zero:

$$\frac{d\sum (A - nD)^2}{dn} = \sum 2D(nD - A)$$

$$= \ 2\sum D(nD - A)$$

$$= \ 2\,(n\sum D^2 - \sum DA) = 0 \quad (7)$$

Hence, deriving *n* from (7):

$$n = \frac{\sum DA}{\sum D^2} \qquad (8)$$

Consequently, the minimum standard deviation of SF for the CI model is:

$$\sigma_{min}^{CI} = \sqrt{\sum (A - D\frac{\sum DA}{\sum D^2})^2/N} \qquad (9)$$

To derive explicit solutions suitable for software processing, like MATLAB, *A* and *D* can be represented as column vectors, and we can express *n* in matrix form as follows:

$$\boldsymbol{n} = \boldsymbol{A^T(D^TD)^{-1}D} \quad (10)$$

By the same token, the minimum standard deviation of SF for the CI model is:

$$\boldsymbol{\sigma_{min}^{CI}} = \sqrt{\sum(\boldsymbol{A - (A^T(D^TD)^{-1}D)D})^2/\boldsymbol{N}} \quad (11)$$

4.1.3 Measurement scopes

The measurements both indoor and outdoor (Figure 12) are done exclusively in a Far Field region, out of the Fresnel Region to ensure the minimal inductive effect and steady and accurate RX power [22]. The following equation is a common way to define an agreed near-field area:

$$Radiating\ Near\ Field\ (Fresnel\ Region) \leq \frac{2D^2}{\lambda} \quad (12)$$

, where D is the largest linear dimension of the Horn antenna and λ is the wavelength.

According to the outline drawing specifications of the 261V-25/385-F horn antenna [23], D is 4.328 cm. Considering frequency to be 60GHz, the Fresnel Region can be found according to Eq. 12:

$$Radiating\ Near\ Field\ (Fresnel\ Region) \leq \frac{2\times0.04328^2}{\frac{3\times10^8}{60\times10^9}} = 0.749\ \text{m}$$

Given that the Far-Field area is next to the Fresnel Region [22], it is expected that the antenna waves will transition into the Far-Field region beyond a distance of 75cm, resulting in stability of the field's inductive effects. Further tests in the far-field area are still in the works.

As can be observed in Figure 11, the RX system remains stationary at the 0 mark (floor markings) in this configuration, while the TX system travels away, ranging from 1m to 10m T – R distance. During both, indoor and outdoor (Figure 12) experiments, The Spectrum Analyzer is set to the same reference level of -45.9 dBm and 30 dB preamplification, which is deducted when defining the actual RX power. 10 measurements of the received power are made at each integer meter of T – R distance during indoor experiments, whereas the outdoor experiments covered the same 8 integer distance measurements, but with measurements at the 4th and 6th meters excluded to reduce the experiment time to minimize the possible equipment damage by cold weather. Also, to minimize the mentioned damage, all equipment including the Spectrum analyzer and DC power supplies were covered with the special polyethylene foam thermal insulation material. The outdoor experiments are conducted at NU campus on February 8, 2024, at 1:00 pm local time in Astana, Kazakhstan. The environmental parameters recorded during the experiment included a temperature of -9°C, relative humidity of 88%, atmospheric pressure measuring 1009.8 millibars, and a wind speed of 18 m/s. The indoor measurements are limited to a maximum of 10 meters because of the limited laboratory space, whereas such limit in the harsh outdoor environment is mainly conditioned by the strong path losses, due to which the RX power is significantly low almost imperceptible, i.e. near the background noise. The measurements in both indoor and outdoor scenarios are done by moving the TX system to an integer meter T – R distance while ensuring complete compliance with the LOS condition using the laser pointer. A minimum of 10 observed RX power values are recorded per each T – R separation distance in both indoor and outdoor measurements. In accordance with the Table 3, the actual RX power is defined as follows:

$$P_{RX} = P_O - 30 + L_{RF2IF} - G_{RX} + L_{LO2RF} + L_W \qquad (13)$$

, where P_O denotes the RX power observed on the spectrum analyzer, 30 refers to the preamplification done by the Spectrum Analyzer, the L_{RF2IF} (RF to IF conversion loss), as well as, L_{LO2RF} (LO-to-RF isolation loss) are the parameters of the I/Q Mixer provided in Table 3, L_W refers to the losses associated with the wires and connectors between the RX system and the Spectrum Analyzer and is around 9.34 dB and Gain denotes the RX antenna gain. The reason for subtracting the preamplification and the antenna gain is that the observed RX power is twice amplified. By the same token, the reason for adding the loss values back is to compensate them to define the actual RX power at the receiving point. The path loss per each distance and each measurement and both for indoor and outdoor scenarios, hence, can be defined as:

$$PL = P_{TX} - P_{RX} \qquad (14)$$

4.2 Measurement Results

4.2.1 Path Loss results presentation

This section describes the results obtained via hardware experiment at 60 GHz mmWave channel in indoor and outdoor environments. The actual RX power plots both for the indoor and outdoor scenarios are provided in Figure 13. Here, the indoor RX power (red plot) sees a steady decline as the T – R distance increases from 1 meter to 10 meters, whereas the decline steepens notably after the 7m T – R distance in the outdoor scenario (blue plot), indicating a different attenuation behavior compared to the indoor scenario. This behavior resembles the exponential model.

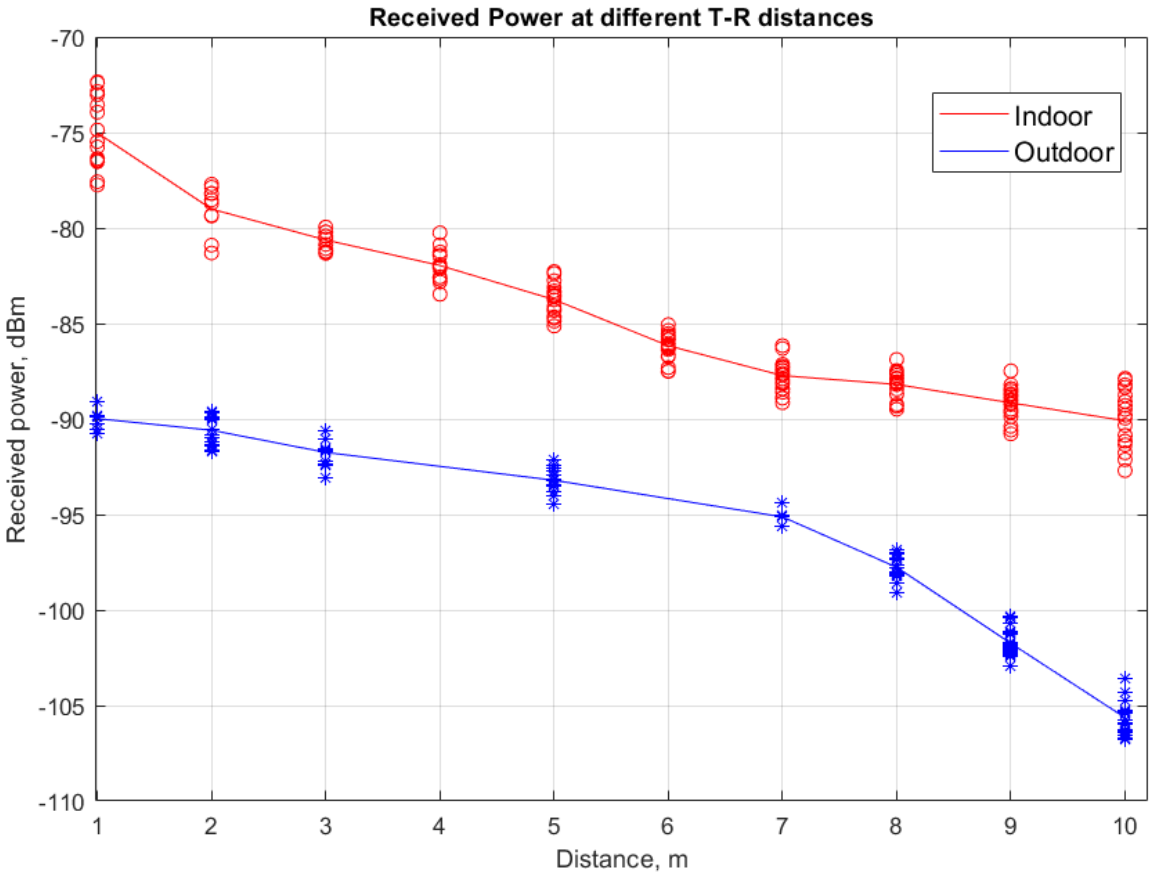

Fig. 13. Actual RX power at Indoor and Outdoor scenarios

Both of the plot lines are drawn through the mean values of the scattered RX measurements per each T – R distance. The obtained measurements are fitted to the CI model provided in Eq. 5 to obtain the PL plots. To do so, first, the A and D parameters of the CI model are defined following Eq. 5. Consequently, the PLE and SF standard deviation showings inherent to the indoor and outdoor cases are obtained utilizing Eqs. 10 and 11 respectively in MATLAB.

The PLE and SF standard deviation values for both of the scenarios are provided in Table 4. The outdoor PLE is about one and a half times larger than the indoor PLE, indicating a more significant attenuation rate in the outside free space during snowstorms than in the indoor environment.

Table 4. PLE and SF parameters

	PLE	σ_{SF}, dB
Indoor	2.77	4.05
Outdoor	4.12	9.32

The PL plots for the indoor and outdoor scenarios are provided in Figures 14 and 15. The respective PL values for both scenarios are obtained using Eq. 14. To generate theoretical PL plots in accordance with Eq. 5 provided in the mentioned figures, relevant SF X_{σ}^{CI} values are obtained using *randn* MATLAB function that can generate normally distributed random numbers with the given standard deviation and zero means. Figures 14 and 15 are depicted simultaneously in Figure 16. As can be noticed from experimental PL plots, the snowstorm has added up to around 15 dB more loss than in the indoor environment at the 1 m T – R separation. This difference has shrunk by around a half closer to the 7 m T – R distance. Finally, the divergence has widened back to 15 dB towards the 10 m T – R distance. On the contrary, the theoretical PL plots for indoor and outdoor scenarios originate from starting PL values that are relatively closer and they diverge as the T – R distance increases. The PLE values for indoor and outdoor scenarios obtained through the MMSE approach (Eq. 10) accounted for 2.77 and 4.12 values, respectively (Table 4). Additionally, acquired standard deviation values of the SF parameter for indoor and outdoor scenarios obtained also through the MMSE approach (Eq. 11) accounted for 4.05 dB and 9.32 dB values, respectively (Table 4). To quantify the exponential nature of the outside path loss, it is modeled using a conventional two-term exponential equation in MATLAB: F(x) = a*exp(b*x) + c*exp(d*x). The two-term exponential model provided a more accurate match compared to the model with just one term. The calculated coefficients, together with their 95% confidence intervals, are shown in Table 5. The fitted curve of the outdoor PL data is presented in Figure 17.

Table 5. 2 term Exponential model coefficients for outdoor PL curve

Coefficient	Value	95% confidence bounds
a	93.49	(93.09, 93.88)
b	0.003276	(-0.001171, 0.007722)
c	0.2663	(-0.1486, 0.6812)
d	0.3903	(0.2647, 0.516)

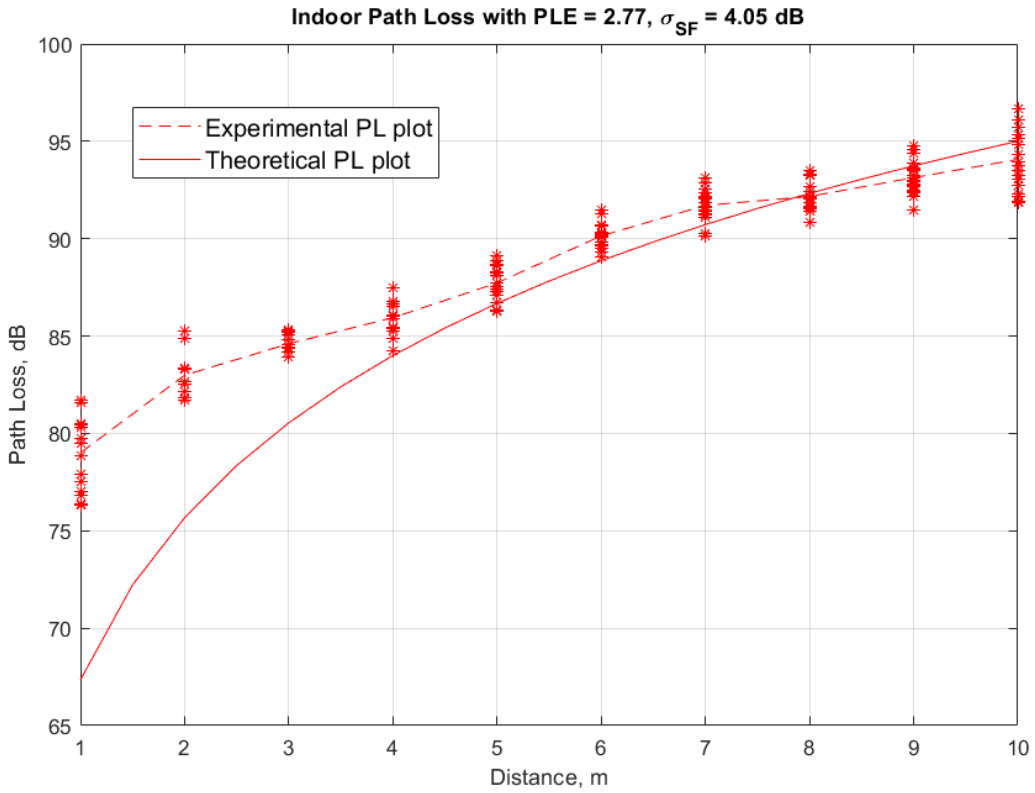

Fig. 14. 60 GHz mmWave indoor PL plot

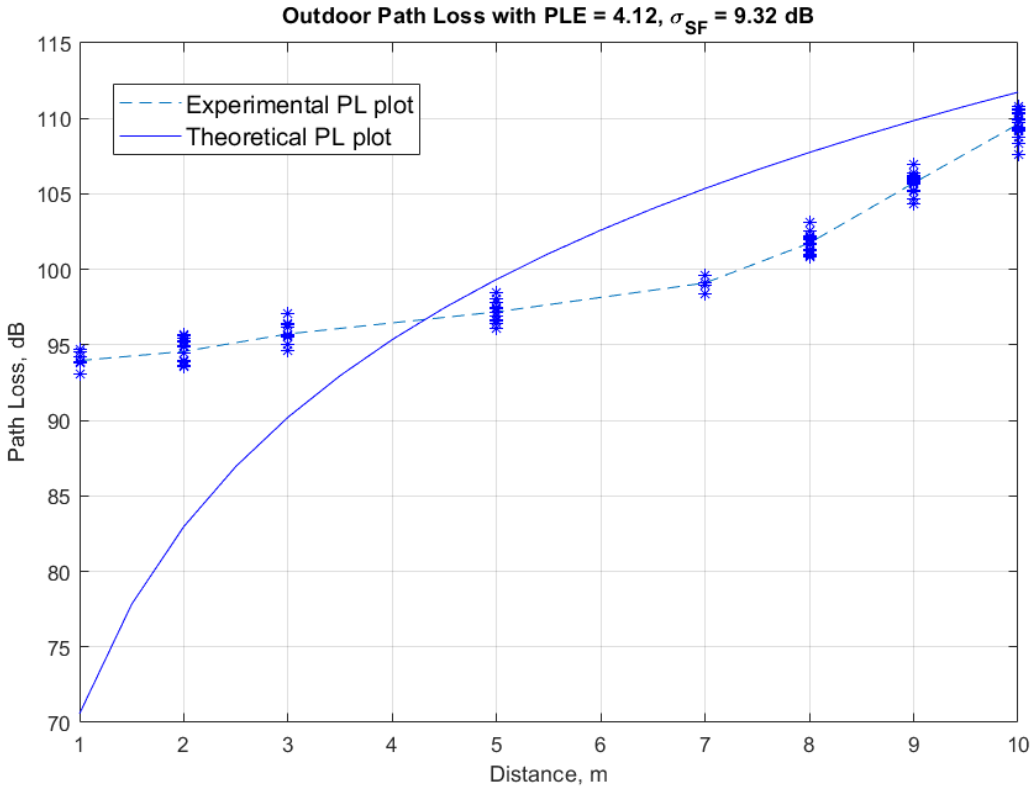

Fig. 15. 60 GHz mmWave outdoor PL plot

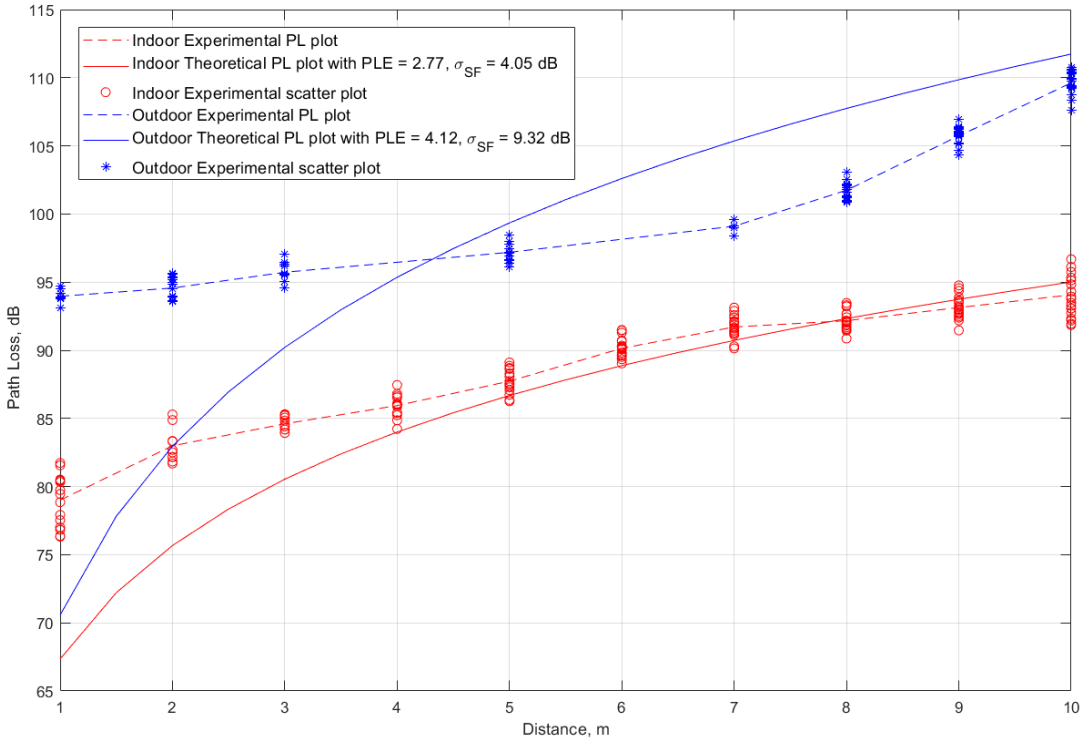

Fig. 16. 60 GHz mmWave combined PL plots

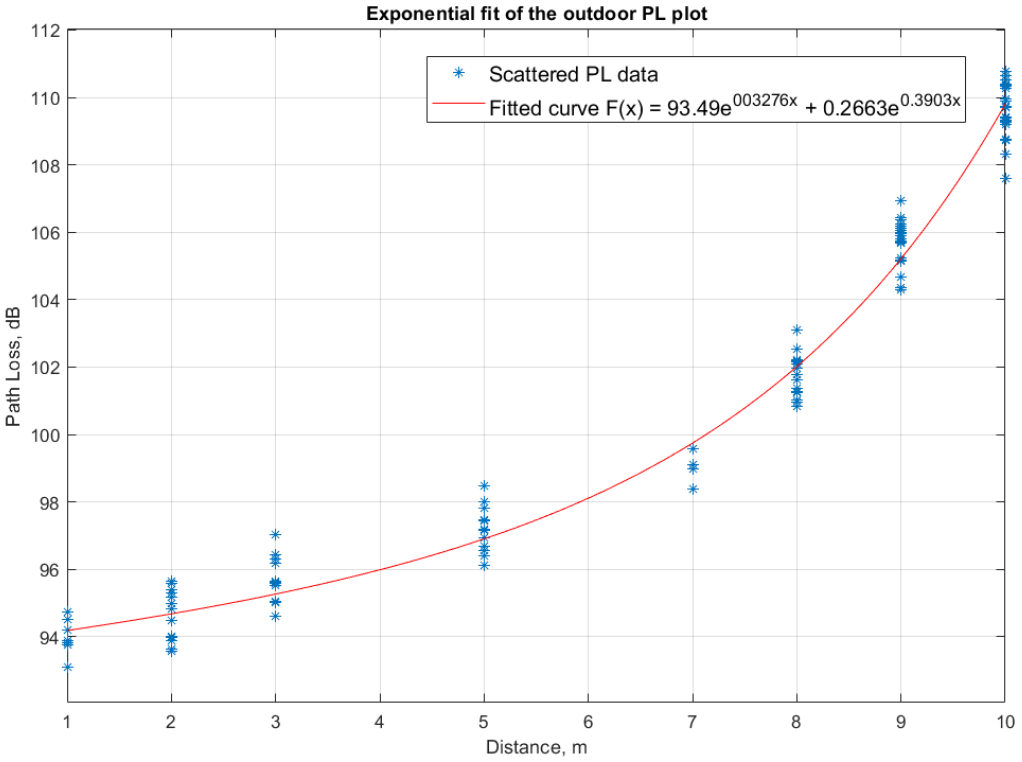

Fig. 17. 60 GHz outdoor PL plot exponential fit

4.2.2 Measurement results discussion

The obtained PLE values for indoor and outdoor scenarios fall into an acceptable range from 2 to 5. Primarily, the results confirm the initial expectations that PL increases as the T – R separation becomes larger. The susceptible mmWave signal encounters obstacles and reflections inherent to the office environment that contribute to signal loss, which can explain a moderate rate of signal attenuation suggested by a PLE value of 2.77. The outdoor PLE of 4.12 is approximately one and a half times larger than the indoor PLE, indicating a more significant attenuation rate in outdoor free space, particularly during snowstorms. The standard deviation of SF in the outdoor scenario (9.32 dB) is higher than in the indoor scenario (4.05 dB), indicating increased variability and unpredictability in signal strength outdoors, most likely owing to terrain irregularities and environmental factors such as snowflakes, buildings, and high wind speed. Experimental path loss plots reveal that the

snowstorm causes around 15 dB higher loss than the indoor environment at a 1-meter T - R separation. This disparity decreases by almost half when the T - R distance reaches 7 meters, but then increases back to 15 dBm again at the 10-meter mark. Several factors may have contributed to the observed differences in the behavior of the wireless channel at 60 GHz mmWave frequencies between indoor and outdoor environments. The high relative humidity of 88% suggests significant moisture content in the atmosphere, which can degrade signal propagation through absorption and scattering mechanisms [2]. Moisture in the air can attenuate mmWave signals, particularly during adverse weather conditions such as snowstorms. The recorded temperature of -9°C, indicating cold weather conditions, can also improve atmospheric moisture content and signal absorption, leading to increased signal attenuation [2]. Moreover, high wind speed of 18 m/s can introduce additional challenges, as it causes random and rapid movement of snowflakes leading to induced higher snow concentration.

The exponential nature of the outdoor Path Loss plot after the 7m T – R separation can be explained by the attenuation due to the snowstorm. In a recent study by Garg and Soni, the effect of snowfall in the Himalayan mountains on signal attenuation at 433 MHz frequency was examined [24]. They deployed four transceiver dipole antennas, constructed together with an Arduino Mini Board, at 100 cm above the snow surface, utilizing one as a source node and the rest three as destination nodes, each in a far-field region from the source node [24]. The measurements were done during the snowfall for 11.5 hours with intervals of 1 minute and by the end of the measurement period, a total of 60 cm of snow had accumulated above the nodes level. The results on recorded received signal strength indicator (RSSI) values suggest that the path loss of the channel could be described by 3rd-order polynomial models if nodes are not buried in the snow [24]. However, as the nodes become buried in snow, path loss can be modeled by the exponential model, and the more they are buried the

better path loss resembles the exponential model [24]. This suggests that with the increase in snow concentration between the TX and RX nodes, the RX power suffers exponential path loss. This may partly explain the transition of the path loss to the exponential behavior beyond the 7m T – R distance, as the obstructing snow gets denser with the TX moving away during the snowstorm with high wind speed. Another study by Nakamura et al. examined the influence of snow accretion on antenna radome on RX power at 45 GHz at different snow moisture contents (5.5%, 10%, and 14.6%) by placing different snow plates with different thicknesses between TX and RX horn antennas [25]. Results show that the RX power sees notable degradation up to 45 dB due to the presence of moisture contained within the snow on the antenna's surface [25]. Hence, the snow accretion on the antenna's surface can be another reason that adds up to the exponential path loss, as by the lapse of time of measurements more snow gets accreted on both antennas. To sum up, this discourse emphasizes the considerable effect of snowfall and its accumulation on signal attenuation and route loss in wireless communication systems operating in outdoor situations. The exponential nature of the path loss observed during snowstorms is attributable to the presence of snow between the TX and RX nodes, with snow density, moisture content, and wind speed all impacting signal deterioration. Understanding these environmental conditions is critical for developing robust and reliable wireless communication systems that can operate efficiently in snow-prone outdoor areas.

Chapter 5 – Simulation with obtained PLE and SF parameters

5.1 Presentation of the simulation results with the obtained PL outdoor parameters

The simulations are repeated for the sake of objective assessment of the factual campus coverage of the 60 GHz mmWave downlink channel with 1 GHz bandwidth, ½ coding rate, and 30 dBm TX power considering the identified PLE and SF parameters for the outdoor snowstorm weather conditions and indoor envirionment. The obtained indoor PLE and SF parameters can be utilized in simulating the outdoor coverage in Astana for the clear sky weather with mild room temperature, since they are comparable with the same parameters for outdoor LOS PL experiments obtained in [15] and [1]. The coverage results with PLE = 4.12, σ_{SF} = 9.32 dB are demonstrated in Table 6 and the coverage results with PLE = 2.77, σ_{SF} = 4.05 dB are demonstrated in Table 7. In the case of simulation results with snowstorm weather PL parameters, as illustrated in Table 6, the coverage of the lowest ordered QPSK mode accounted for 2.26% of the LOS area of the base stations, as well as 1.25% and 0.26% for 16-QAM and 256-QAM modulation modes, respectively. The coverage contour and the SNR CDF plots per each modulation mode of the 60 GHz channel with snowstorm PL parameters are shown in Figures 18 and 19, respectively. As for the results with indoor PL parameters, shown in Table 7, the coverage of the QPSK mode is around 28% of the total LOS region. The coverage has shrunk to 10.29% and 1.81% in 16-QAM and 256-QAM modulation mode cases, respectively. The coverage contour and the SNR CDF plots of the 60 GHz channel with indoor PL parameters are shown in Figures 20 and 21, respectively.

Table 6. The percentage of Line-of-Sight (LOS) area covered by each mode of modulation at 60 GHz signal with PLE = 4.12, σ_{SF}=9.32 dB

QPSK	2.26%
16-QAM	1.25%
256-QAM	0.26%

Table 7. The percentage of Line-of-Sight (LOS) area covered by each mode of modulation at 60 GHz signal with PLE = 2.77, σ_{SF}=4.05 dB

QPSK	28.02%
16-QAM	10.29%
256-QAM	1.81%

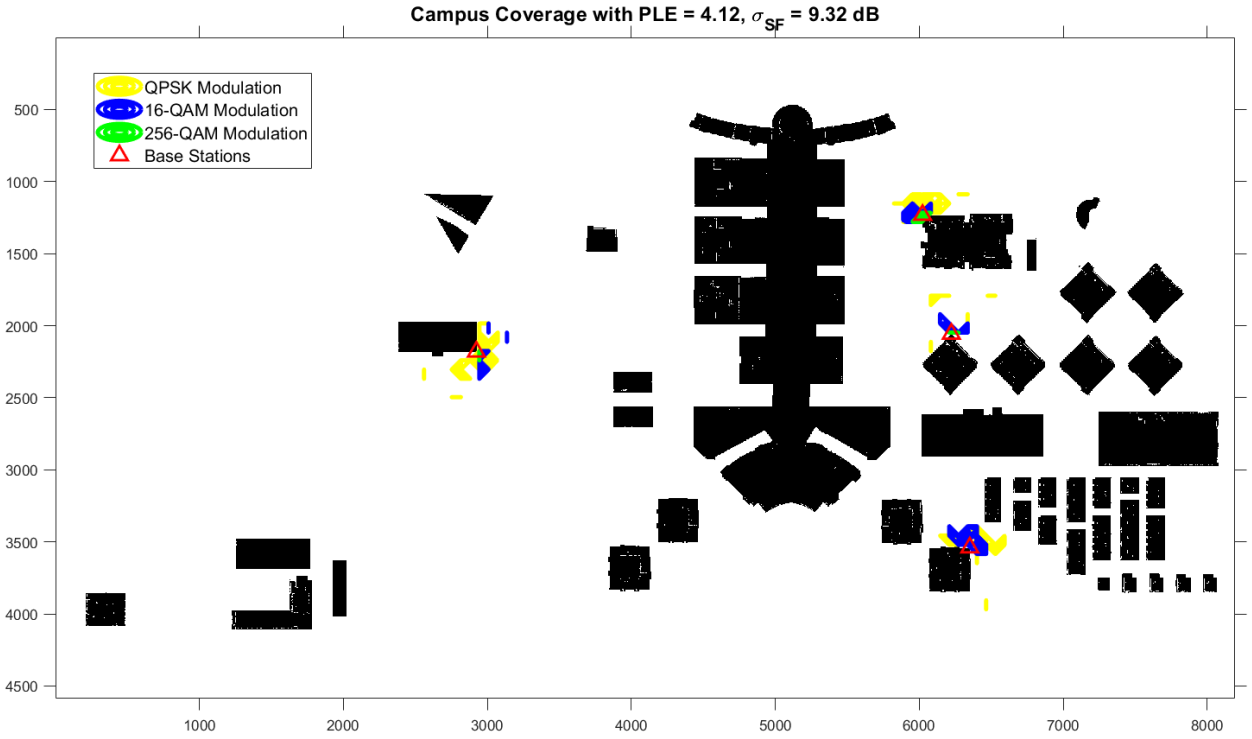

Fig. 18. Received Power Contour for the 60 GHz channel with PLE = 4.12, σ_{SF} = 9.32 dB

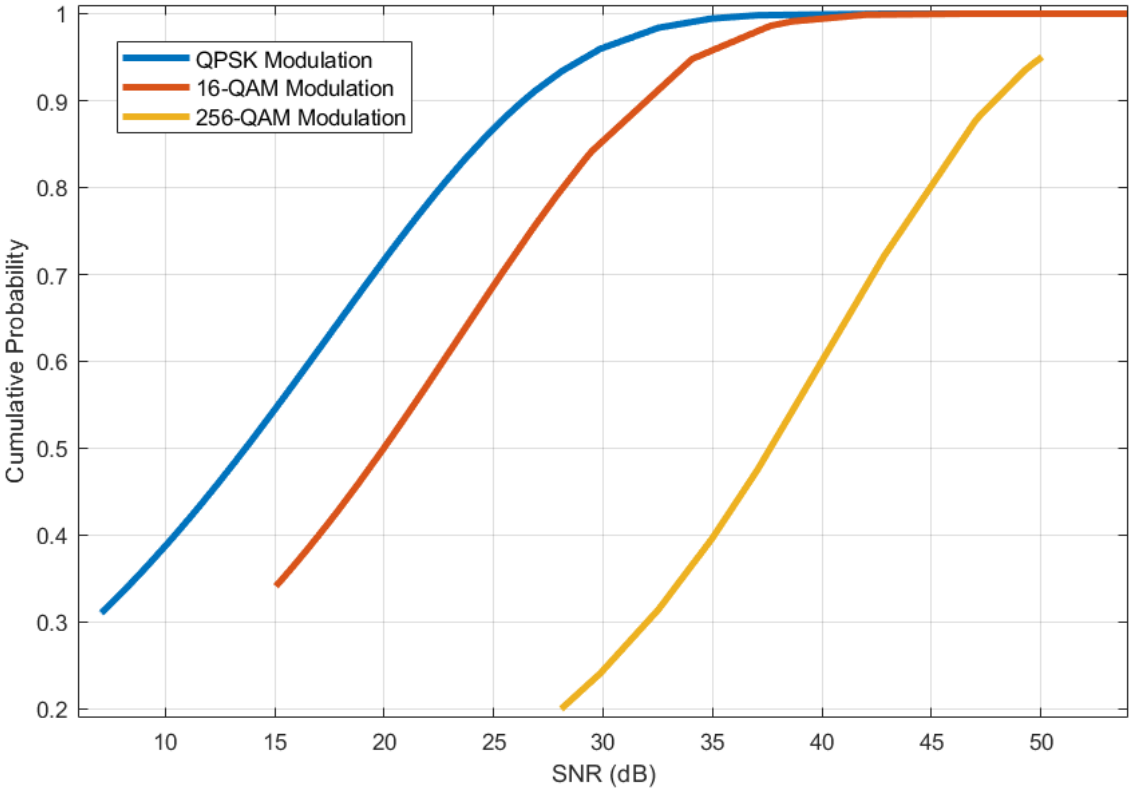

Fig. 19. SNR CDF for the 60 GHz channel with PLE = 4.12, σ_{SF} = 9.32 dB

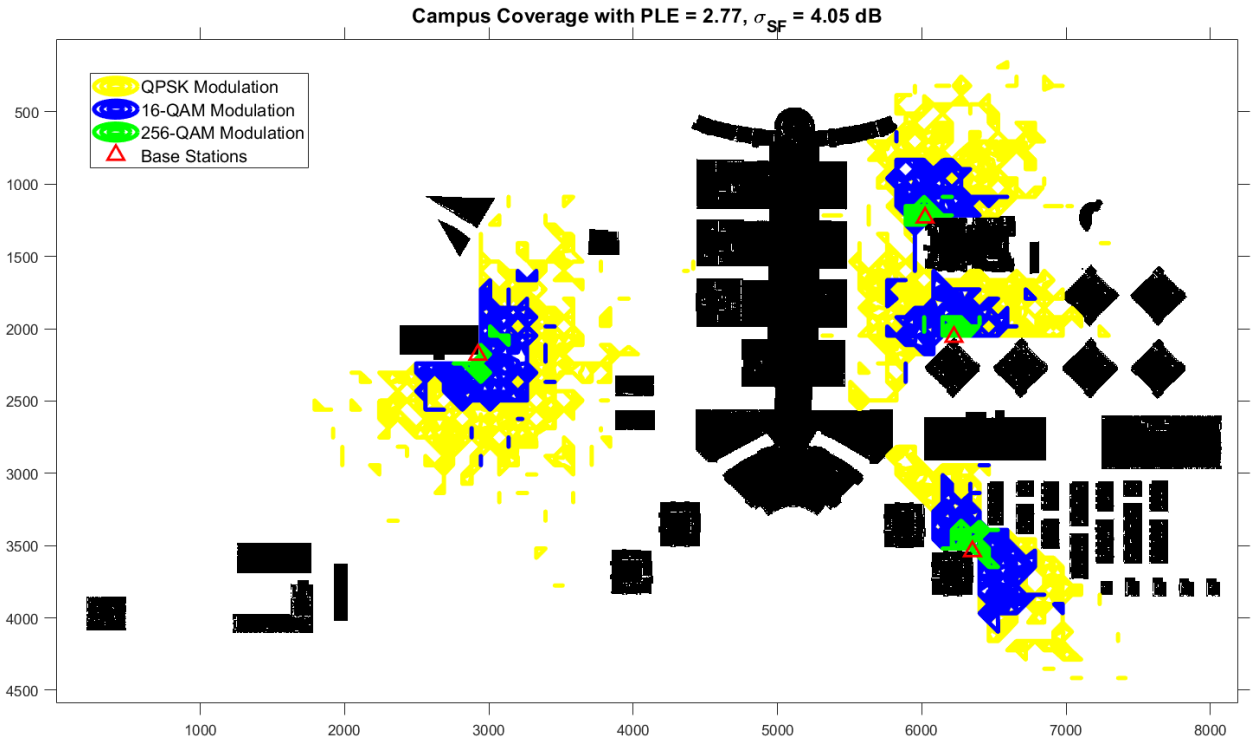

Fig. 20. Received Power Contour for the 60 GHz channel with PLE = 2.77, σ_{SF} = 4.05 dB

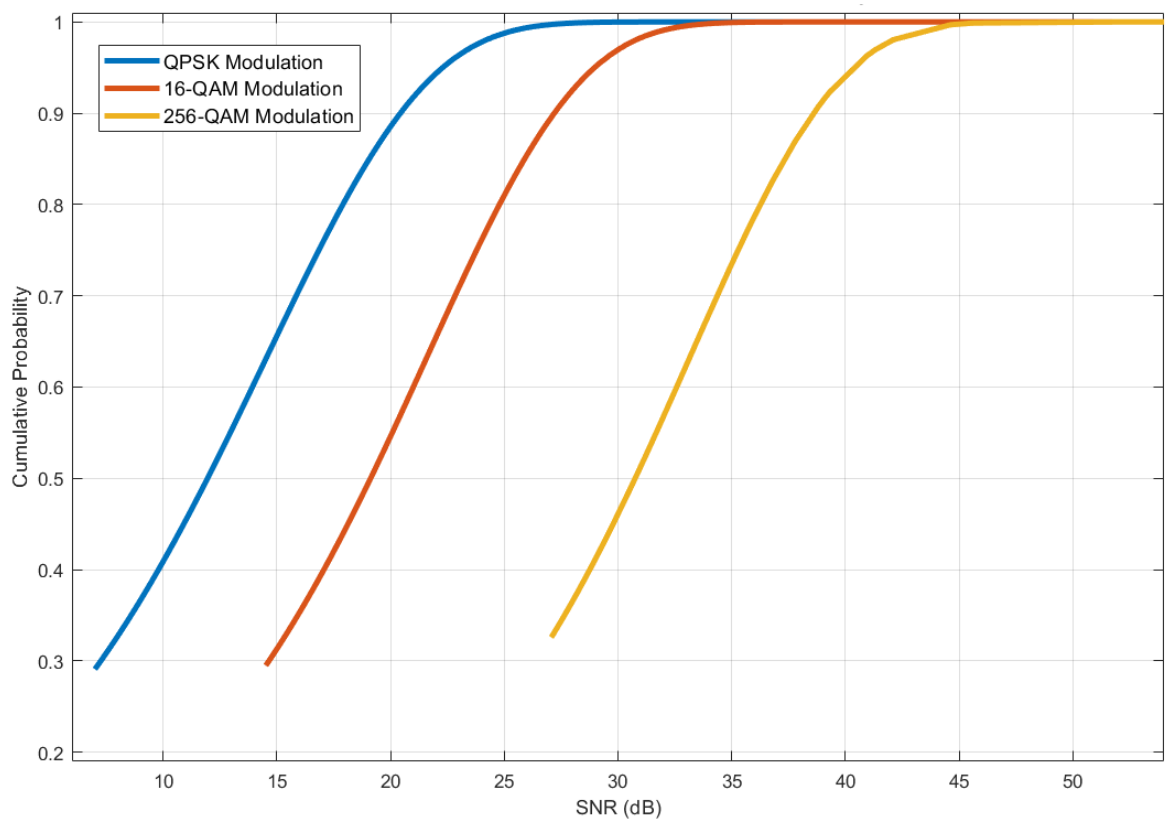

Fig. 21. SNR CDF for the 60 GHz channel with PLE = 2.77, σ_{SF} = 4.05 dB

5.2 Discusion of the simulation results with the obtained PL outdoor parameters

The obtained new set of simulation results incorporates environmental parameters such as temperature of -9°C, relative humidity of 88%, atmospheric pressure of 1009.8 millibars, and wind speed of 18 m/s, which affect the path loss exponent (PLE) and shadow fading (SF) parameters utilized in the simulations. These parameters are specific to outdoor snowstorm weather conditions and have a notable impact on coverage results. These results provide meaningful perspectives on how a 60 GHz downlink mmWave channel would behave in harsh weather conditions, particularly in a snowstorm. Unlike the theoretical circumstances with minimal FSPL PLE of 2, the second set of simulation results demonstrate lower coverage percentages across all modulation modes (QPSK, 16-QAM, and 256-QAM) for the 60 GHz mmWave downlink channel under snowstorm weather conditions. The coverage percentages are significantly lower compared to the LOS area of the considered BSs. As can

be noted in Figure 18, the SF factor has notably contributed to the coverage percentage due to the random nature of the appearance of the signal blind places even in close and complete LOS vicinities. The intermittent or discontinuous pattern of the RX power contour for every modulation mode is conditioned by the earlier mentioned SF phenomenon due to humidity and snowflake absorption which explains how the path loss of the channel may become larger for a random value with zero mean and standard deviation of 9.32 dB. Nevertheless, the major part in limiting the LOS area is primarily attributed to the high path loss exponent value of 4.12, which comprehensively characterizes the overall channel capability to restrict the scope of mmWave channel communication in power aspects. It is because besides contour patterns being discontinuous, on top of that they are also limited by small coverage areas, hence the coverage percentages at 60 GHz reduced to inappreciable amounts (Table 6). In metric scale, they are equivalent to a neighborhood of around 35 meters, 20 meters, and 10 meters in radius, respectively, which is poor performance in the sense of outdoor coverage by the mmWave channel. The coverage percentage in comparison with the previous simulation has reduced by 97.74%, 98.58%, and 98% in QPSK, 16-QAM, and 256-QAM modulation modes, respectively. As for the results around simulations with indoor PL parameters (Figure 20), the coverage is appreciably larger than in the case of snowstorm. The coverage of the LOS region in the latter case is 12, 8 and 7 times larger than coverage in snowstorm environment for QPSK, 16-QAM and 256-QAM modulation modes respectively. Nevertheless, as compared with the coverage results of the 60 GHz channel for the PLE = 2 shown in Figure 6 and stated in Table 2, the obtained coverage results are still significantly deteriorated. Moreover, remembering that the simulator utilizes 2D distance instead of 3D, it is crucial to note that these results are already positively biased compared to the real coverage.

Concerning the SNR CDF plots of the snowstorm scenario, in 256-QAM modulation, if the 50-percentile SNR value accounted for 30 dB in the previous 60 GHz simulation

(Figure 9), this time it has increased up to 37 dB (Figure 19), implying considerable decline in the number of vertices having valid signal. If the steady-state SNR value (~ 100–percentile) for both the QPSK and 16-QAM modes in the previous simulation is achieved at approximately 35 dB (Figure 9), in Figure 19 the respective value is around 45 dB. Regarding the SNR CDF plots with the indoor PL parameters, also a perceptiple right shift is observed in Figure 21 compared to Figure 9 in case of 256-QAM modulation mode. However, the SNR CDF plots with the related to the rest modulation modes have seen notable left shift. In general, with an increase in PLE and SF standard deviation parameters, the SNR plots become more inclined, meaning the slope of the plots decreases. Overall, these observed right shifts imply that the number of vertices having high-valued SNRs decreases on top of the decrease in the number of vertices that meet the required SNR limit, yet the latter decrease rate is higher than the former. To sum up, these simulations have proven the mmWave channels' performance can be impractical in harsh weather conditions unless exogenous interventions, such as relay base stations and beamforming technology [19], are introduced. Moreover, the coverage in conditions of clear sky conditions with near-room temperature can also be practically insufficient for large outdoor territories like the NU campus, considering that simulations are positively biased since 2D distances are significantly lower than the 3D distances from BSs mounted on the roofs of 7 and 12-story dormitory buildings.

Chapter 6 – Conclusion

6.1 Simulator inferences

Although limited by 2D distance measurement, the campus coverage simulation results provide useful information about the performance of several frequency bands and modulation methods for outdoor communication on the NU campus. The findings highlight the importance of carrier frequency on coverage, with higher frequencies resulting in reduced coverage due to increasing path loss. Specifically, at 60 GHz and 73 GHz, coverage for all modulation orders considerably declines compared to the 28 GHz range. This reduction is due to a legitimate rise in path loss at higher frequencies, emphasizing the importance of frequency selection in outdoor communication systems. Furthermore, the simulation results demonstrate the effect of modulation order on coverage area inside LOS zones. While QPSK gives 100% LOS coverage across all frequency bands and increasing modulation orders result in steadily decreasing coverage, this increase triggers an abrupt decline in coverage for 256-QAM modulation. The distribution of SNR values over the campus area provides valuable information about signal quality at various frequency bands and modulation rules. The findings show that when modulation order and frequency increase, SNR distributions move to the left, suggesting that maximum SNR values drop. Given the trade-offs between data rate and coverage area, lesser modulation orders such as QPSK and 16-QAM provide larger LOS coverage, but higher modulation orders such as 256-QAM result in significant coverage decreases. However, 256-QAM has the best bandwidth efficiency of any modulation method, making it ideal for high data rate transmission, especially in densely populated regions with significant user traffic. Recognizing the performance benefits of QPSK modulation in tough settings and for longer BS-user distances, 16-QAM and 256-QAM modulation schemes are recommended for high data rate communication in constrained areas, particularly in the mmWave band. Furthermore, the simulation demonstrates the potential use of various

modulation strategies depending on geographical factors. In highly populated locations with significant user activity, the highest modulation order may be preferable. QPSK mode, on the other hand, may provide acceptable coverage in locations with lower population density due to its larger coverage. Furthermore, given Astana's adverse weather conditions, QPSK and 16-QAM modes, which are less susceptible to noise and distortion, are preferred for reliable performance during the winter.

6.2 Hardware experiments

The hardware tests at the 60 GHz mmWave channel in both indoor and outdoor locations provide important insights into signal propagation properties, especially in adverse weather circumstances like snowstorms. The observed RX power behavior and path loss plots reveal unique attenuation patterns across indoor and outdoor circumstances, with snowstorms worsening signal deterioration in outdoor environments. The experimental results show that outdoor environments, particularly during snowstorms, exhibit much greater signal attenuation than indoor conditions. The outdoor PLE is around one and a half times bigger than the inside PLE, indicating a higher attenuation rate in open space, especially under severe weather conditions.

Due to environmental factors including topographical irregularities, precipitation, buildings, and strong winds, the standard deviation of SF is also greater outside, indicating greater signal strength volatility and unpredictability. The presence of snow between the nodes highlights the exponential trend in the outdoor path loss plot, particularly when the distance between the transmitter and receiver exceeds 7 meters. According to earlier mentioned research, signal attenuation increases exponentially with increase in snow concentration; the rate of deterioration is usually determined by snow concentration, moisture content, and wind speed. Prior studies have established that the accumulation of precipitation

and snow on antenna surface has a detrimental effect on the signal strength of outdoor wireless communication systems. Receiving power can be significantly diminished by the existence of snow between antennas; signal loss can be attributed to both the density and moisture content of the snow. Comprehending these environmental circumstances is of the utmost importance to design and implement dependable and resilient wireless communication systems that can operate effectively in wintry outdoor settings and account for the combined impacts of snowfall, wind, and precipitation.

6.3 Repeated simulation with PL parameters

By objectively examining the campus coverage of the 60 GHz mmWave downlink channel during wintry weather conditions through repetitive simulations utilising the obtained outside PLE and SF parameters, crucial insights are gained into the practical PL limitations encountered by mmWave communication systems. The coverage of these models, which incorporate defined PLE and SF characteristics that are unique to outdoor snowfall conditions, is considerably reduced in comparison to idealised theoretical scenarios. The coverage findings show significant decreases in all modulation modes (QPSK, 16-QAM, and 256-QAM) at 60 GHz mmWave frequencies. Coverage percentages for base stations' LOS areas drop to tiny fractions - 2.26%, 1.25%, and 0.26% for QPSK, 16-QAM, and 256-QAM, repspectively. These minimal coverage regions highlight the impracticality of using mmWave channels for outdoor communication during snowstorms. In terms of simulation findings with indoor PL settings, the coverage is significantly greater than during snowfall. According to the results using indoor PL values reported in Table 7, the QPSK mode covers approximately 28% of the whole LOS zone. The coverage has changed to 10.29% and 1.81% in the 16-QAM and 256-QAM modulation modes, respectively. Nonetheless, coverage in clear sky conditions with near-room temperatures may be insufficient for large outdoor territories such as the NU

campus as well, given that simulations are positively biased because the utilized 2D distances are significantly lower than 3D distances from BSs mounted on the roofs of 7 and 12-story dormitory buildings.

The analysis of the SNR CDF plots emphasizes the difficulty encountered by harsh weather conditions. The rightward shifts in SNR distributions indicate a decrease in the number of vertices with valid signals, which is particularly noticeable in 256-QAM modulation mode. Steady-state SNR values for QPSK and 16-QAM modes also show significant increases, indicating prolonged high attenuation owing to snowfall conditions. Overall, our simulations demonstrate the impracticality of using mmWave channels for outdoor communication under adverse weather situations such as snowstorms. The severe losses in coverage and poor SNR distributions indicate the necessity for exogenous interventions such as relay base stations and beamforming technologies to improve the resilience and reliability of mmWave communication networks in harsh environments.

6.4 Future work and Concluding remarks

Further study is required to assess traffic patterns and determine the optimal configuration of base stations and modulation types to successfully deliver high-traffic connections in outdoor regions of the campus. In addition, to obtain more accurate and practical PL simulator results, the campus map needs to be updated with the buildings' height, so the distance parameter would consider 3D distance, instead of 2D approximation. Future research shall also consider combining directional antennas with sectorized cells rather than the uniform circular and omnidirectional antenna array used in this study as BS, to improve and make both PL and network traffic analysis more accurate. Moreoever, the employed "brute force" technique making 36068 RX power calculations and comparisons should be improved in the future to use dynamic or greedy algorithms to decrease the number of

redundant computations, comparisons, and assignments. This may be required and may allow for more efficient time management when the number of BS rises. As per the hardware experiments, to minimize the effect of the snow moisture on antenna radiation in accordance with the study in [25], the antennas shall be placed under high canopies which would not interfere with the antenna radiation pattern and harbor the antennas from snowfall. This could allow us to obtain more precise inferences on how snowfall affects the PL.

In summary, mmWave technology has the promise of high-speed wireless communication; nevertheless, its practical use in outdoor environments requires advanced mitigation techniques to address the challenges posed by adverse weather conditions, such as snowstorms. To fully realize the potential of mmWave communication systems in practical applications, further study and technological advancements are needed. To sum up, this thesis research provides a comprehensive analysis of outdoor communication systems, offering profound insights into the complex interactions between signal properties, ambient circumstances, modulation schemes, and frequency ranges. This research contributes to the ongoing quest for robust and reliable outdoor communication systems that are suitable for practical uses by addressing significant difficulties and outlining potential areas for advancement.

References

[1] T. S. Rappaport *et al*., "Millimeter Wave Mobile Communications for 5G Cellular: It Will Work!," in *IEEE Access*, vol. 1, pp. 335-349, 2013, doi: 10.1109/ACCESS.2013.2260813.

[2] J. Karjalainen, M. Nekovee, H. Benn, W. Kim, J. Park and H. Sungsoo, "Challenges and opportunities of mm-wave communication in 5g networks", *2014 9th International Conference on Cognitive Radio Oriented Wireless Networks and Communications (CROWNCOM)*, pp. 372- 376, 2014, doi: 10.4108/icst.crowncom.2014.255604.

[3] G. R. MacCartney and T. S. Rappaport, "73 GHz millimeter wave propagation measurements for outdoor urban mobile and backhaul communications in New York City," *2014 IEEE International Conference on Communications (ICC)*, Sydney, NSW, Australia, 2014, pp. 4862- 4867, doi: 10.1109/ICC.2014.6884090.

[4] T. E. Bogale and L. B. Le, "Massive MIMO and mmWave for 5G Wireless HetNet: Potential Benefits and Challenges," in *IEEE Vehicular Technology Magazine*, vol. 11, no. 1, pp. 64-75, March 2016, doi: 10.1109/MVT.2015.2496240.

[5] K. Du, O. Ozdemir, F. Erden and I. Guvenc, "28 GHz Indoor and Outdoor Propagation Measurements and Analysis at a Regional Airport," *2021 IEEE 32nd Annual International Symposium on Personal, Indoor and Mobile Radio Communications (PIMRC)*, Helsinki, Finland, 2021, pp. 866-872, doi: 10.1109/PIMRC50174.2021.9569260.

[6] H. Zhao *et al*., "28 GHz millimeter wave cellular communication measurements for reflection and penetration loss in and around buildings in New York city," *2013 IEEE International Conference on Communications (ICC)*, Budapest, Hungary, 2013, pp. 5163-5167, doi: 10.1109/ICC.2013.6655403.

[7] Hao Xu, V. Kukshya and T. S. Rappaport, "Spatial and temporal characteristics of 60-GHz indoor channels," in *IEEE Journal on Selected Areas in Communications*, vol. 20, no. 3, pp. 620- 630, April 2002, doi: 10.1109/49.995521.

[8] "Study on channel model for frequencies from 0.5 to 100 GHz", 3rd Generation Partnership Project (3GPP) Technical report TR 38.901 V16.1.0 Release 16, [online] Available: http://www.3gpp.org/DynaReport/38901.htm.

[9] "Measurement results and final mmmagic channel models", Technical report, [online] Available: https://5g-mmmagic.eu/results/.

[10] G. R. MacCartney and T. S. Rappaport, "Rural Macrocell Path Loss Models for Millimeter Wave Wireless Communications," in *IEEE Journal on Selected Areas in Communications*, vol. 35, no. 7, pp. 1663-1677, July 2017, doi: 10.1109/JSAC.2017.2699359.

[11] Y. Shen, Y. Shao, L. Xi, H. Zhang and J. Zhang, "Millimeter-Wave Propagation Measurement and Modeling in Indoor Corridor and Stairwell at 26 and 38 GHz," in *IEEE Access*, vol. 9, pp. 87792-87805, 2021, doi: 10.1109/ACCESS.2021.3081822.

[12] S. Ju, Y. Xing, O. Kanhere and T. S. Rappaport, "Millimeter Wave and Sub-Terahertz Spatial Statistical Channel Model for an Indoor Office Building," in *IEEE Journal on Selected Areas in Communications*, vol. 39, no. 6, pp. 1561-1575, June 2021, doi: 10.1109/JSAC.2021.3071844.

[13] Zhu Wen *et al*., "mmWave channel sounder based on COTS instruments for 5G and indoor channel measurement," *2016 IEEE Wireless Communications and Networking Conference Workshops (WCNCW)*, Doha, 2016, pp. 37-43, doi: 10.1109/WCNCW.2016.7552672.

[14] T. S. Rappaport, F. Gutierrez, E. Ben-Dor, J. N. Murdock, Y. Qiao and J. I. Tamir, "Broadband Millimeter-Wave Propagation Measurements and Models Using Adaptive-Beam Antennas for Outdoor Urban Cellular Communications," in *IEEE Transactions on Antennas and Propagation*, vol. 61, no. 4, pp. 1850-1859, April 2013, doi: 10.1109/TAP.2012.2235056.

[15] S. Sun, G. R. MacCartney, M. K. Samimi, S. Nie and T. S. Rappaport, "Millimeter wave multi-beam antenna combining for 5G cellular link improvement in New York City," *2014 IEEE International Conference on Communications (ICC)*, Sydney, NSW, Australia, 2014, pp. 5468- 5473, doi: 10.1109/ICC.2014.6884191.

[16] J. Liang, Y. Wang, D. Xie and Y. Jing, "Analysis and Optimization of Weak Coverage of LTE Network in Universities," *2022 IEEE 10th Joint International Information Technology and Artificial Intelligence Conference (ITAIC)*, Chongqing, China, 2022, pp. 344-349, doi: 10.1109/ITAIC54216.2022.9836525.

[17] M. T. Moayyed, F. Restuccia and S. Basagni, "Comparative Performance Evaluation of mmWave 5G NR and LTE in a Campus Scenario," *2020 IEEE 92nd Vehicular Technology Conference (VTC2020-Fall)*, Victoria, BC, Canada, 2020, pp. 1-5, doi: 10.1109/VTC2020-Fall49728.2020.9348727.

[18] S. Askarov, R. C. Kizilirmak and I. A. Ukaegbu, "Path Loss Analysis and System Coverage for 28 GHz, 60 GHz and 73 GHz Band Wireless Communication Systems," *2023 IEEE 17th International Conference on Application of Information and Communication Technologies (AICT)*, Baku, Azerbaijan, 2023, pp. 1-4, doi: 10.1109/AICT59525.2023.10313166.

[19] J. S. Kim *et al*., "System Coverage and Capacity Analysis on Millimeter-Wave Band for 5G Mobile Communication Systems with Massive Antenna Structure", *International Journal of Antennas and Propagation*, vol. 2014, Article ID 139063, 11 pages, 2014. https://doi.org/10.1155/2014/139063

[20] T. Tuovinen, N. Tervo and A. Pärssinen, "Analyzing 5G RF System Performance and Relation to Link Budget for Directive MIMO," in *IEEE Transactions on Antennas and Propagation*, vol. 65, no. 12, pp. 6636-6645, Dec. 2017, doi: 10.1109/TAP.2017.2756848.

[21] G. R. Maccartney, T. S. Rappaport, S. Sun and S. Deng, "Indoor Office Wideband Millimeter-Wave Propagation Measurements and Channel Models at 28 and 73 GHz for Ultra-Dense 5G Wireless Networks," in *IEEE Access*, vol. 3, pp. 2388-2424, 2015, doi: 10.1109/ACCESS.2015.2486778.

[22] "The Near-Field vs. Far-Field Regions of an Antenna," *cadence*. https://resources.system-analysis.cadence.com/blog/msa2021-the-near-field-vs-far-field-regions-of-an-antenna

[23] "V-Band Standard Gain Horn Antennas | WR-15 | 50–75 GHz," *miwv.com*. Available: https://www.miwv.com/v-band-standard-gain-horn-antennas-wr-15-50-75-ghz-5/.

[24] Garg, R.K. and Soni, S.K. (2022), "Empirical path loss models at 433 MHz in Himalayan snow for health monitoring", *World Journal of Engineering*, vol. 19 no. 2, pp. 157-165. https://doi.org/10.1108/WJE-03-2021-0134

[25] K. Nakamura, N. Iwasawa, K. Kawasaki, S. Yoshida, and M. Takahashi, 'The Attenuation Characteristics of Millimeter-wave by Snow Accretion', *IEICE Communications Express*, vol. 9, 10 2020, doi:10.1587/comex.2020XBL0128